SIAM J. Appl. Math.
Vol. 75, No. 2, pp. 443–467

AVIAN INFLUENZA DYNAMICS UNDER PERIODIC ENVIRONMENTAL CONDITIONS*

NAVEEN K. VAIDYA† AND LINDI M. WAHL‡

Abstract. Since wild birds are the major natural reservoir for all known influenza A viruses, understanding the ecology of avian influenza (AI) viruses circulating in wild birds is critical to predicting disease risk in wild and domestic birds and preventing transmission to humans. AI virus which is shed by infected birds into aquatic environments plays a pivotal role in the sustained transmission of AI. Recent laboratory experiments, however, show that viral persistence in water is highly sensitive to environmental conditions such as temperature, which varies seasonally and geographically. Here, we develop mathematical models to study the effects of time-varying environmental conditions on AI dynamics, deriving the effects of temperature on the basic reproductive number ($\mathcal{R}_0$), the final outbreak size, and the effective reproductive number ($\mathcal{R}_e$). For periodic environmental temperatures, we derive a mathematical formulation of an AI invasion threshold ($\mathcal{R}_i$) and conclude that apart from the mean temperature, the amplitude of the periodic temperature profile plays a significant role in the invasion of wild bird populations by AI. In particular, both higher means and higher amplitudes (warmer and more variable temperatures) reduce the likelihood of AI invasion. We also analyze the global dynamics of the model proving that AI is uniformly persistent in the wild bird population if $\mathcal{R}_i > 1$. In numerical work, we fit the model to recent experimental data and field survey data from Northern Europe. Two important and robust quantitative conclusions emerge: that direct transmission is negligible compared to indirect and that immunity wanes within about 4 weeks. The latter conclusion is of particular interest since many previous models assume lifetime immunity. We also demonstrate that time-varying temperature may be the underlying cause of several features of AI dynamics which are observed in real data. In particular, AI prevalence is observed to peak in spring and fall but to wane in summer; this behavior naturally emerges from our model under a wide range of conditions.

Key words. aquatic wild birds, avian influenza, direct bird-to-bird transmission, immunity, indirect fecal-oral transmission, invasion threshold, reproductive number, time-varying environment, periodic system

AMS subject classifications. 34D20, 37N25, 92B05, 92D30, 92D40

DOI. 10.1137/140966642

1. Introduction.

Avian influenza virus (AIV) has become an important public health issue because aquatic birds constitute the major natural reservoir of all influenza A viruses, including the highly pathogenic H5N1 AIV transmitted to humans [23, 38, 45, 67]. In particular, birds belonging to *Anseriformes* (ducks, geese, and swans) and *Charadriiformes* (gulls, terns, and waders) have been reported to be efficient hosts of AIV with a rich pool of genetic and antigenic diversity [67, 69], important factors in cross-species transmission. Such cross-species transmission events from birds to humans usually bring significant risks of mortality; for example, one million people died in the 1968 influenza pandemic [37], and almost 50% of infected people died in H5N1 outbreaks in Africa, Asia, Europe, and the Middle East [68]. Better understanding of the ecology of low pathogenic AIV and its dynamics in aquatic wild

*Received by the editors April 28, 2014; accepted for publication (in revised form) December 22, 2014; published electronically March 19, 2015. This work was funded by the Natural Sciences and Engineering Research Council of Canada.

http://www.siam.org/journals/siap/75-2/96664.html

†Department of Mathematics and Statistics, University of Missouri-Kansas City, Missouri, 64110 (vaidyan@umkc.edu). This author's work was supported by start-up funds from the University of Missouri–Kansas City and a UMRB grant from the University of Missouri Research Board.

‡Department of Applied Mathematics, Western University, London, Ontario N6A 5B7, Canada (lwahl@uwo.ca).

birds will be critical in predicting influenza dynamics in the human population and devising control strategies.

In birds, influenza viruses preferentially infect cells lining the intestinal tract [43]. During the infectious period of about 1 week (range 6–10 days) [9, 36, 43, 67], infected birds excrete virus particles in high concentrations in their feces. Interestingly, these viruses can be highly stable in water and remain infective even for several months [10, 11, 55, 56, 66]. Upon ingestion, susceptible birds become infected by viruses that persist in water. This transmission mechanism, via the indirect fecal-oral route, is extremely efficient and thought to be the primary cause of influenza infection in wild aquatic birds [11, 32, 33, 66]. Importantly, the persistence of influenza virus in water depends sensitively on environmental factors such as temperature, pH, and salinity [10, 11, 14, 55, 66], indicating that environmental factors might strongly influence disease dynamics.

While extensive surveillance studies have been conducted on AIV in wild birds from different parts of the world [15, 22, 24, 26, 29, 30, 35, 38, 39, 43, 44, 46, 49, 52, 59, 64], only limited mathematical models of influenza dynamics among wild birds have been explored [5, 6, 7, 8, 31, 49, 50]. A simple SIR (susceptible, infected, recovered) model was analyzed in Henaux, Samuel, and Bunck [31] and Roche et al. [49]; the model was further extended to incorporate more than one AIV strain [5, 7]. Migration is a common strategy for birds occupying seasonal habitats, such as *Anseriformes* and *Charadriiformes*, and may play a significant role in the transmission of AIV [45]; migration has also been considered in some models [6, 8]. These models have contributed substantially to our understanding of the importance of bird migration and fecal-oral transmission for avian influenza (AI) in wild birds. Nonetheless several important features of AI dynamics remain poorly understood. In particular, the prevalence and peak time of AI among wild birds vary widely, location to location as well as year to year [43, 45]. Likewise, double peaks of influenza prevalence during the summer and fall of a single breeding season have been observed [43]. These common features of AI have not been captured by existing models, raising the question of whether environmental variation plays a role in these observed prevalence patterns.

Using stochastic models, two recent studies [8, 50] have clearly highlighted the importance of environmental effects in AIV transmission and their implications for pathogen invasion. In a model with migration, Breban et al. [8] considered the effect of environmental heterogeneity on virus prevalence by taking two different virus decay rates for the breeding ground and wintering ground. However, recent laboratory experimental evidence suggests that the fluctuations in environmental conditions which occur even within a few weeks can substantially alter virus infectivity [11, 14, 55, 67]. As yet, the predicted effects of these time-varying environmental conditions on AI dynamics in wild bird populations remain unexplored.

Our approach is outlined as follows. In section 2 we propose a mathematical model of low pathogenic AI (LPAI) dynamics that includes both time-varying environmental effects and seasonal migration. In particular, the effects of continuous seasonal variation in water temperature are included in the model. In section 3, we examine how environmental factors affect the basic reproductive number, the effective reproductive number, and the final outbreak size. For periodic conditions representing the environmental temperature, we derive an AI invasion threshold and study how this threshold criterion is sensitive to the mean and the amplitude of the temperature profile. Furthermore, we provide a global analysis of AI dynamics to derive an AI persistence criteria. In section 4, we find meaningful parameter values by fitting the model to experimental data measuring AI persistence in water and to field data

tracking AI prevalence in migratory waterfowl in Northern Europe, including a sensitivity analysis. We compute numerical estimates of the basic reproductive numbers and final outbreak size and examine their temperature sensitivity. We also perform a statistical comparison against other models which do not allow for temperature variation. Finally, in section 5 we explore several questions of ecological and epidemiological interest, for example, the balance of direct versus indirect transmission in AI, and the duration of acquired immunity. We also explore the effects of temperature variation on both single-season and long-term prevalence patterns.

2. The model.

2.1. One-season-one-ground model. We derive the one-season-one-ground (OSOG) model by incorporating environmental effects into a simple SIR-type model [49, 61]. A schematic diagram of the model is shown in Figure 1. The aquatic wild bird population is divided into three mutually exclusive compartments: susceptible birds (S), infected birds (I), and recovered birds (R). We further consider a compartment V that measures the concentration of AIV in a water source. We describe the disease dynamics using the following differential equations:

$$\frac{dS}{dt} = -\beta_d IS - \beta_i VS - dS + \eta R, \quad S(0) = S_0, \tag{2.1}$$

$$\frac{dI}{dt} = \beta_d IS + \beta_i VS - \gamma I - dI, \quad I(0) = I_0, \tag{2.2}$$

$$\frac{dR}{dt} = \gamma I - dR - \eta R, \quad R(0) = R_0, \tag{2.3}$$

$$\frac{dV}{dt} = pI - \Omega(E(t))V, \quad V(0) = V_0. \tag{2.4}$$

The units of our state variables S, I, and R are numbers of individuals. The model includes two possible mechanisms of virus transmission: (a) direct bird-to-bird transmission proportional to susceptible birds, S, and infected birds, I, at a rate β_d, and (b) indirect fecal-oral transmission proportional to susceptible birds, S, and virus concentration in water, V, at a rate β_i. Note that since our main objective is to evaluate the effects of a time-varying environment, which appears only in the environmental virus degradation term (equation (2.4)), we use mass action terms for both direct and indirect transmission in the analytical work to follow, as suggested by Tien and Earn [61]. However, in the numerical results we also test the model fit under an assumption of frequency-dependent transmission [8, 49].

Infected birds shed virus particles at rate p and these virus particles decay in water at rate Ω, as described in the subsection to follow. Parameters d, γ, and η represent the natural death rate, the recovery rate, and the rate of immunity loss, respectively. Since LPAI does not cause severe disease in wild birds [45], we have not considered death due to disease in our model. We assume annual, pulsed reproduction (see the two-seasons-two-grounds (TSTG) model below) such that the births of new susceptibles are included in the initial conditions of the OSOG model.

2.2. Environmental effect, $\Omega(E)$. As mentioned in the introduction, the persistence of infectious AIV particles in aquatic environments is critical to the transmission of this disease. We introduce this effect via dependence of the viral decay rate, Ω, on environmental factors, $E(t)$, such as the temperature, pH, and salinity of water. In particular, we assume that if a viral particle is still infectious, it decays in time interval Δt with probability $\Omega(E(t))\Delta t$, and this probability changes with, for

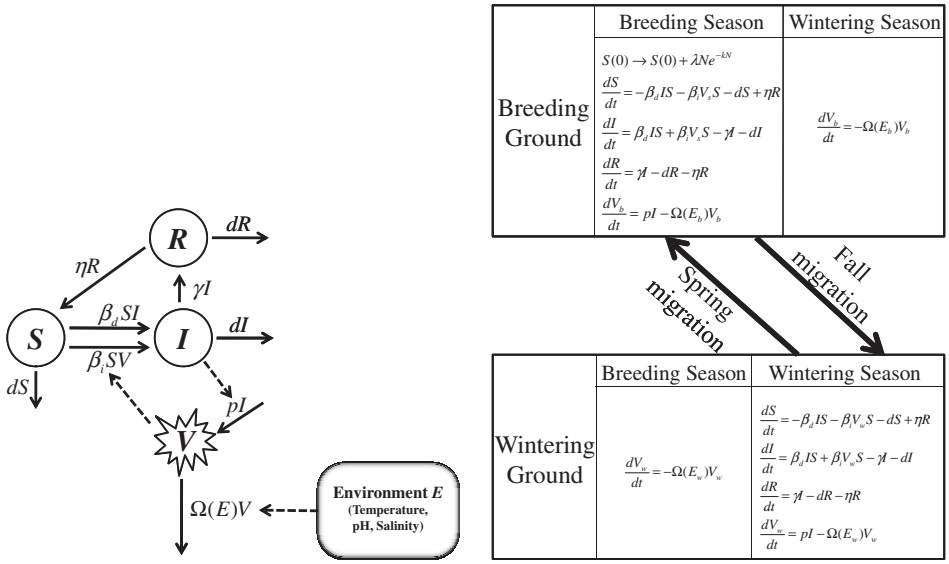

FIG. 1. *Schematic diagram of* (a) *the OSOG model and* (b) *the TSTG model for AIV dynamics in wild birds. In* (a)*, solid arrows represent the rate of flow of the bird or virus population, while the dashed arrows represent causes for corresponding solid arrows.*

example, temperature. The incorporation of environmental variation over time is the important novel feature of our model. As we shall show later, this change in the environment, particularly in temperature, can have significant impacts on AI dynamics, AI invasion, and AI persistence.

Recent experimental estimates of Ω and meaningful parameter values are explained more fully in section 4. Since the sensitivity of Ω to temperature is higher than pH and salinity, we focus on temperature variation, unless otherwise stated, which can be approximated by a periodic function with a period of 1 year. We will also use the notation $\Omega(E(t)) = \bar{\Omega}$ to denote a reduced model in which the environmental decay rate of AIV is assumed constant.

2.3. Two-seasons-two-grounds model. To understand the long-term dynamics of the disease it is essential to consider two seasons and two grounds, since for many AIV-endemic species, birds migrate to spend time in two different grounds (the breeding ground and the wintering ground) in two different seasons (the breeding season and the wintering season) [43, 45, 64]. Birds breeding in one geographic region are observed to follow a similar migration path yearly [1, 45] and return yearly to known breeding and wintering sites [2]. Usually birds leave the breeding ground and move to the wintering ground in mid fall and return to the breeding ground in early spring.

To address this behavior mathematically, we use two systems of the OSOG model, one in the breeding ground (subscript b) and one in the wintering ground (subscript w). The connection between the two is an impulsive change at fixed times. In particular, if the wintering season begins at time t_w, we take $S_w(t_w) = S_b(t_w^-)$ and $S_b(t_w) = 0$, with similar equations for the I and R populations. If the breeding season begins at time t_b, we take $S_b(t_b) = S_w(t_b^-)$ and $S_w(t_b) = 0$. There is no impulsive change in the virus concentration, $V_b(t_w) = V_b(t_w^-)$, and likewise for V_w. In the breeding ground system, the environmental variable $E(t)$ is replaced by $T_b(t)$, the time-varying breeding ground temperature; likewise we use $T_w(t)$ in the wintering ground system.

For simplification, we neglect stopovers during migration and the time required to migrate. In the numerical results to follow, we consider a duration of 8 months in the breeding ground and 4 months in the wintering ground; however, our results are not sensitive to this choice. Furthermore, we assume pulsed reproduction, i.e., a density-dependent number of new susceptible birds given by $\lambda N e^{(-kN)}$ are added to the flock at the beginning of each breeding season [8], thus implying $S_b(t_b) = S_w(t_b^-) + \lambda N e^{(-kN)}$. Here, N, λ, and k are the total number of birds, the fecundity constant, and the density-dependent survival rate, respectively. The basic idea of the model considered here is similar to the one in Breban et al. [8], but our model uses a simpler mass action mechanism for new infections and, importantly, includes time-varying periodic environmental effects in both breeding and wintering grounds. Moreover, we do not assume permanent immunity; in fact, we demonstrate in section 4 that waning immunity is a necessary feature of the model in order to mimic the AI prevalence patterns observed in field data from Northern Europe. A schematic diagram of the TSTG model is shown in Figure 1.

3. Analytical results.

3.1. The basic reproductive number. The basic reproductive number, $\mathcal{R}_0$, is defined as the average number of secondary infections generated by a single infected individual introduced into a completely susceptible population. For a location where environmental temperature remains approximately constant over a season, $\mathcal{R}_0$ is a key threshold parameter that indicates—in the deterministic limit—if an epidemic dies out or a disease outbreak occurs, depending upon whether its value exceeds one [3]. Using the next-generation matrix approach [16, 62], we can derive the basic reproductive number for the OSOG model with a constant viral decay rate $\bar{\Omega}$. The model system (2.1)–(2.4) has exactly one disease-free equilibrium $X_0 = (S_0, 0, 0, 0)$, and equations for the infectious and virus compartments of the linearized system at X_0 take the form

$$\frac{dI}{dt} = (\beta_d S_0 - \gamma - d)I + \beta_i S_0 V, \tag{3.1}$$

$$\frac{dV}{dt} = pI - \bar{\Omega} V. \tag{3.2}$$

We introduce the following matrices:

$$\mathcal{F} = \begin{pmatrix} \beta_d S_0 & \beta_i S_0 \\ 0 & 0 \end{pmatrix}, \quad \mathcal{V} = \begin{pmatrix} \gamma + d & 0 \\ -p & \bar{\Omega} \end{pmatrix}.$$

These expressions give

$$\mathcal{F}\mathcal{V}^{-1} = \begin{pmatrix} \frac{\beta_d S_0}{\gamma + d} + \frac{\beta_i p S_0}{(\gamma + d)\bar{\Omega}} & \frac{\beta_i S_0}{\bar{\Omega}} \\ 0 & 0 \end{pmatrix}.$$

Then $\mathcal{R}_0$ corresponds to the spectral radius of $\mathcal{F}\mathcal{V}^{-1}$:

$$\mathcal{R}_0 = \rho(\mathcal{F}\mathcal{V}^{-1}) = \mathcal{R}_0^d + \mathcal{R}_0^i,$$

where $\mathcal{R}_0^d = (\beta_d S_0)/(\gamma + d)$ and $\mathcal{R}_0^i = (\beta_i p S_0)/((\gamma + d)\bar{\Omega})$; these terms represent the number of secondary infections contributed by direct bird-to-bird transmission and indirect fecal-oral transmission, respectively. This expression indicates that even when direct transmission is low ($\mathcal{R}_0^d < 1$), depending on the environmental factors, $\bar{\Omega}$, the contribution $\mathcal{R}_0^i$ from fecal-oral transmission could allow $\mathcal{R}_0$ to exceed one, resulting in disease outbreaks.

3.2. Final outbreak size. For a short-term disease outbreak, the OSOG model system can be approximated by a system without births and deaths ($d = 0$) and without loss of immunity ($\eta = 0$). In this case, disease outbreaks, which occur with $\mathcal{R}_0 > 1$, will eventually die out, as stated in the following lemma.

LEMMA 3.1. *Let $d = \eta = 0$ and $\mathcal{R}_0 > 1$ in the OSOG model system. Then $I(t) \to 0$ and $V(t) \to 0$ as $t \to \infty$.*

Proof. As $d = \eta = 0$, the OSOG model implies $dN/dt = 0$, i.e., $S(t)+I(t)+R(t) = N(t) = N_0$, a constant, and $dS/dt \leq 0$, i.e., $S(t)$ is decreasing. Since $S(t)$ is bounded below by 0, $\lim_{t\to 0} S(t) = \hat{S} \geq 0$. Now, with an initial condition (S_0, I_0, R_0, V_0), consider the solution trajectory, Υ, of the OSOG model, and its omega limit set, Γ_Υ. Again, consider the solution trajectory to the OSOG model with any point $(\bar{S}_0, \bar{I}_0, \bar{R}_0, \bar{V}_0)$ in Γ_Υ as the initial condition. Since the omega limit set is invariant and $\bar{S}_0 = \hat{S}$, $dS/dt = 0$ within Γ_Υ, i.e., $S(\beta_d I + \beta_i V) = 0$ within Γ_Υ. This gives $dI/dt = -\gamma I, I(0) = \bar{I}_0 \Rightarrow I(t) = \bar{I}_0 e^{-\gamma t}$. By the invariance property of Γ_Υ, $\bar{I}_0 = \bar{I}_0 e^{-\gamma t} \forall t$. This implies $\bar{I}_0 = 0$, which gives $dV/dt = -\bar{\Omega} V, V(0) = \bar{V}_0$, and with a similar argument, we get $\bar{V}_0 = 0$. Therefore, the omega limit set, Γ_Υ, consists of the point with $\bar{I}_0 = \bar{V}_0 = 0$. Hence, $I(t) \to 0$ and $V(t) \to 0$ as $t \to \infty$. ∎

For further insight into an AI outbreak, it is useful to evaluate the final outbreak size $\mathcal{Z}$, defined as the proportion of the population that is eventually infected by a newly invading AIV. Following the approach of Tien and Earn [61], we can estimate the final outbreak size for an AI outbreak using the result presented in the following proposition.

PROPOSITION 3.2. *Let $d = \eta = 0$, and let $\mathcal{R}_0 > 1$ for the OSOG model system (2.1)–(2.4). Then the final outbreak size, $\mathcal{Z}$, satisfies the relation*

$$\mathcal{G}(\mathcal{Z}) = 1 - \mathcal{Z} - \exp\left(-\mathcal{R}_0 \mathcal{Z} - \frac{\beta_i V_0}{\bar{\Omega}}\right) = 0. \tag{3.3}$$

Proof. A function $\Xi(t)$, defined by

$$\Xi(t) = \log S(t) + \left(\frac{\beta_d}{\gamma} + \frac{\beta_i p}{\gamma \bar{\Omega}}\right) R(t) - \frac{\beta_i}{\bar{\Omega}} V(t),$$

remains constant along solution trajectories of the OSOG model system (2.1)–(2.4). Using $\lim_{t\to\infty} S(t) = \hat{S}$, $\lim_{t\to\infty} R(t) = \hat{R}$, $\lim_{t\to\infty} I(t) = 0 = \lim_{t\to\infty} V(t)$ (Lemma 3.1), and $S(t) + I(t) + R(t) = N_0$, we get

$$\lim_{t\to\infty} \Xi(t) = \log\left(N_0 - \hat{R}\right) + \left(\frac{\beta_d}{\gamma} + \frac{\beta_i p}{\gamma \bar{\Omega}}\right) \hat{R}.$$

Since $\Xi(t)$ remains constant along solution trajectories, $\lim_{t\to\infty} \Xi(t) = \Xi(0)$. This gives

$$\log\left(\frac{N_0 - \hat{R}}{S_0}\right) + \left(\frac{\beta_d}{\gamma} + \frac{\beta_i p}{\gamma \bar{\Omega}}\right)(\hat{R} - R_0) + \frac{\beta_i}{\bar{\Omega}} V_0 = 0.$$

Now, assuming the population is almost entirely susceptible at the beginning, i.e., $S_0 \to N_0$, and so $I_0 \to 0, R_0 \to 0$, and using $R_0 \to 0 \Rightarrow \hat{R}/N_0 \to \mathcal{Z}$, we get relation (3.3). ∎

3.3. The effective reproductive number. While $\mathcal{R}_0$ calculated above is useful to identify an environmental temperature that ensures that the epidemic does not grow at the beginning of the season, an epidemic later in the season may not be avoided because of temperature variations. To study the effect of temperature over the entire season, a more relevant measure is the effective reproductive number, $\mathcal{R}_e(t)$. $\mathcal{R}_e(t)$ measures the average number of infectious birds resulting from a single infective bird introduced at time t into the population, given the susceptible population at that time [13, 18]. For the OSOG model, $\mathcal{R}_e(t)$ is given by

$$\mathcal{R}_e(t) = \frac{\beta_d S(t)}{\gamma + d} + \frac{\beta_i p S(t)}{(\gamma + d)\Omega(T(t))}.$$

3.4. AI invasion threshold. Despite being a useful indicator for both the risk of an epidemic and the effort required to control the epidemic, one of the weaknesses of $\mathcal{R}_e(t)$ is that this number is not a threshold parameter for disease invasion [65]. We now derive an AI invasion threshold, $\mathcal{R}_i$, using an approach similar to those of Wang and Zhao [65] and Liu, Zhao, and Zhou [40].

For our τ-periodic OSOG model system, i.e., $\Omega(t+\tau) = \Omega(T(t+\tau)) = \Omega(T(t)) = \Omega(t)$, with $\tau = 365$ days, equations for the infectious and virus compartments of the linearized system at the disease free equilibrium, X_0, take the form

$$\frac{dI}{dt} = (\beta_d S_0 - \gamma - d)I + \beta_i S_0 V, \tag{3.4}$$

$$\frac{dV}{dt} = pI - \Omega(t)V. \tag{3.5}$$

We consider

$$\mathcal{F}_\tau = \begin{pmatrix} \beta_d S_0 & \beta_i S_0 \\ 0 & 0 \end{pmatrix}, \quad \mathcal{V}_\tau(t) = \begin{pmatrix} \gamma + d & 0 \\ -p & \Omega(t) \end{pmatrix}.$$

We assume that $Y(t,s)$, $t \geq s$, is the evolution operator of the linear τ-periodic system

$$\frac{dy}{dt} = -\mathcal{V}_\tau(t)y. \tag{3.6}$$

That is, for each $s \in \mathbb{R}$, the 2×2 matrix $Y(t,s)$ satisfies

$$\frac{d}{dt}Y(t,s) = -\mathcal{V}_\tau(t)Y(t,s) \quad \forall t \geq s, Y(s,s) = I,$$

where I is the 2×2 identity matrix. Then the monodromy matrix $\Phi_{-\mathcal{V}_\tau}(t)$ of (3.6) is equal to $Y(t,0), t \geq 0$.

Let $\varphi(s)$, τ-periodic in s, be the initial distribution of infectious individuals. Then $\mathcal{F}_\tau\varphi(s)$ is the rate of new infections produced by the infected individuals who were introduced at time s. Given $t \geq s$, then $Y(t,s)\mathcal{F}_\tau\varphi(s)$ represents the distribution of those infected individuals who were newly infected at time s and remain in the infected compartments at time t.

Let C_τ be the ordered Banach space of all τ-periodic functions from $\mathbb{R}$ to $\mathbb{R}^2$, with the maximum norm $||\cdot||$ and the positive cone $C_\tau^+ := \{\varphi \in C_\tau : \varphi(t) \geq 0 \ \forall t \in \mathbb{R}\}$. We now define a linear operator $\mathcal{L} : C_\tau \to C_\tau$ by

$$(\mathcal{L}\varphi)(t) = \int_0^\infty Y(t, t-\xi)\mathcal{F}_\tau\varphi(t-\xi)d\xi \quad \forall t \in \mathbb{R}, \varphi \in C_\tau.$$

Here, $\int_0^\infty Y(t,t-\xi)\mathcal{F}_\tau\varphi(t-\xi)d\xi = \int_{-\infty}^t Y(t,s)\mathcal{F}_\tau\varphi(s)ds$ gives the distribution of accumulative new infections at time t produced by all those infected individuals $\varphi(s)$ at time previous to t. Therefore, $\mathcal{L}$ is the next infection operator [65], and we define an AI invasion threshold as $\mathcal{R}_i = \rho(\mathcal{L})$, the spectral radius of $\mathcal{L}$.

As in Wang and Zhao [65] and Liu, Zhao, and Zhou [40], we let $\mathcal{T}(t,\vartheta)$ be the monodromy matrix of the linear τ-periodic system

$$\frac{d\tau}{dt} = \left(-\mathcal{V}_\tau(t) + \frac{1}{\vartheta}\mathcal{F}_\tau\right)\tau, \quad t \in \mathbb{R},$$

with parameter $\vartheta \in (0,\infty)$. Since $\mathcal{F}_\tau$ is nonnegative and $-\mathcal{V}_\tau(t)$ is cooperative, it follows that $\rho(\mathcal{T}(\tau,\vartheta))$ is continuous and nonincreasing in $\vartheta \in (0,\infty)$, and $\lim_{\vartheta\to\infty}\rho(\mathcal{T}(\tau,\vartheta)) < 1$. Thus, as proved in Wang and Zhao [65], we have the following two results.

LEMMA 3.3. *The following statements hold* [65].

(i) *If $\rho(\mathcal{T}(\tau,\vartheta)) = 1$ has a positive solution ϑ_0, then ϑ_0 is an eigenvalue of operator $\mathcal{L}$, and hence $\mathcal{R}_i > 0$.*

(ii) *If $\mathcal{R}_i > 0$, then $\vartheta = \mathcal{R}_i$ is the unique solution of $\rho(\mathcal{T}(\tau,\vartheta)) = 1$.*

(iii) *$\mathcal{R}_i = 0$ if and only if $\rho(\mathcal{T}(\tau,\vartheta)) < 1$ $\forall\vartheta > 0$.*

LEMMA 3.4 (see [65]). *The disease-free equilibrium X_0 is locally asymptotically stable if $\mathcal{R}_i < 1$ and unstable if $\mathcal{R}_i > 1$.*

In addition to the condition $\mathcal{R}_i < 1$, we are also able to obtain an explicit condition under which the solution of the linearized system (3.4)–(3.5) satisfies $(I(t),V(t)) \to 0$ as $t \to \infty$.

LEMMA 3.5. *If $\mathcal{R}_0^d < 1$ and $Q(t) < 1$ $\forall t \in \mathbb{R}$, where*

$$Q(t) = p\beta_i S_0 \int_{-\infty}^t e^{-(\gamma+d-\beta_d S_0)(t-s)} \int_{-\infty}^s \exp\left(-\int_{\bar{s}}^s \Omega(\bar{\bar{s}})d\bar{\bar{s}}\right) d\bar{s}ds,$$

then $(I(t),V(t)) \to 0$ as $t \to \infty$.

Proof. For the proof, see Appendix A. ∎

Note that in the case when $\Omega(t) = \bar{\Omega}$, a constant viral decay rate, we obtain $Q(t) = p\beta_i S_0/(\bar{\Omega}(\gamma + d - \beta_d S_0)) = \bar{Q}$ and, by the above result, if $\bar{Q} < 1$, then the disease-free equilibrium is asymptotically stable. Moreover, it can easily be verified that for $\mathcal{R}_0^d < 1$, $\bar{Q} < 1 \Leftrightarrow \mathcal{R}_0 < 1$.

3.5. Global dynamics: AI persistence. To understand AI eradication or long-term AI persistence in wild birds, we need to consider recruitment or birth of new susceptible birds. While we assume annual, pulsed reproduction in the TSTG model (section 2), equivalently, for analysis purposes, we add a constant bird recruitment rate $\Lambda = dS_0$ to (2.1) assuming that the bird population is in steady state before AIV is introduced. Using $N(t) = S(t) + I(t) + R(t)$, the total bird population, we obtain the following system equivalent to system (2.1)–(2.4):

$$\frac{dS}{dt} = \Lambda - \beta_d IS - \beta_i VS - (\eta + d)S + \eta(N - I), \quad S(0) = S_0, \tag{3.7}$$

$$\frac{dI}{dt} = \beta_d IS + \beta_i VS - (\gamma + d)I, \quad I(0) = I_0, \tag{3.8}$$

$$\frac{dN}{dt} = \Lambda - dN, \quad N(0) = N_0, \tag{3.9}$$

$$\frac{dV}{dt} = pI - \Omega(t)V, \quad V(0) = V_0. \tag{3.10}$$

System (3.7)–(3.10) has exactly one disease-free equilibrium $X_0 = (\Lambda/d, 0, \Lambda/d, 0)$. By deriving a condition for the global stability of X_0 in the following theorem, we establish a condition for global eradication of AI from the wild birds.

THEOREM 3.6. *If $\mathcal{R}_i < 1$, then the unique disease-free equilibrium, $X_0 = (\Lambda/d, 0, \Lambda/d, 0)$, is globally asymptotically stable.*

Proof. For the proof, see Appendix B. □

Using techniques similar to the ones by Wang and Zhao [65] and Liu, Zhao, and Zhou [40], we can also prove that $\mathcal{R}_i > 1$ provides a condition for long-term AI persistence in wild birds with at least one positive periodic solution. We state the result in the following theorem.

THEOREM 3.7. *If $\mathcal{R}_i > 1$, then there exists a $\delta > 0$ such that any solution $(S(t), I(t), N(t), V(t))$ of system (3.7)–(3.10) with initial value $(S_0, I_0, N_0, V_0) \in \mathbb{D}_0 = \{(S, I, N, V) \in \mathbb{D} : I > 0, V > 0\}$, where $\mathbb{D} = \{(S, I, N, V) \in \mathbb{R}^4_+ : S + I + R \leq N\}$, satisfies*

$$\liminf_{t\to+\infty} I(t) \geq \delta, \quad \text{and} \quad \liminf_{t\to+\infty} V(t) \geq \delta,$$

and system (3.7)–(3.10) admits at least one positive periodic solution.

Proof. For the proof, see Appendix C. □

In the following section, we use the derivations outlined above to examine the temperature sensitivity of the basic reproductive number, the effective reproductive number, the final outbreak size, and the invasion threshold at parameter values estimated from both experimental and field data.

4. Numerical results.

4.1. Environmental decay rate. A strength of our approach is that recent experimental data allows for accurate quantitative estimates of the decay of infectious AIV over time, in aquatic environments. In particular, the relationship $\Omega(E)$ is derived from laboratory experimental data [11], in which the time required for the infectivity of AIV in water to be reduced by 90% was recorded for seven temperatures, eight pH values, and seven salinities. For each of three datasets, we transformed the time for infectivity to be reduced by 90% to the log scale. For simplicity, we considered polynomials to fit the data and chose a curve with the least degree that reasonably fits the data. We note that this step simply allows for interpolation between experimentally measured points; the choice of different polynomial functions does not change our results. As shown in Figure 2, we used a constant function, a linear function, and a quadratic function for salinity variation, temperature variation, and pH variation, respectively. The resulting curves (Figure 2) give relationships between the time to reduce infectivity by 90% (i.e., 1 $\log_{10}$) and water temperature, pH, and salinity. We assume that AIV infectivity in water decreases over time at a log-linear rate [10, 55]. This provides the following relationships:

$$\begin{array}{rlll} \text{Temperature:} & E = T, & \Omega(T) & = (\log_e 10) e^{(-a_T T - b_T)}; \\ \text{pH value:} & E = A, & \Omega(A) & = (\log_e 10) e^{(-a_A A^2 - b_A A - c_A)}; \\ \text{Salinity:} & E = \zeta, & \Omega(\zeta) & = (\log_e 10) e^{-a_\zeta}. \end{array}$$

Although we provide these relationships for pH and salinity, as explained previously we focus on periodic temperature variations in this contribution. In brief, we take a period of 1 year in the function $T(t) = T_0(1 + \epsilon \sin(\omega t + \phi))$ for time-varying temperature, i.e., $\omega = 2\pi/365$. We fit this periodic function $T(t)$ to monthly averaged temperature

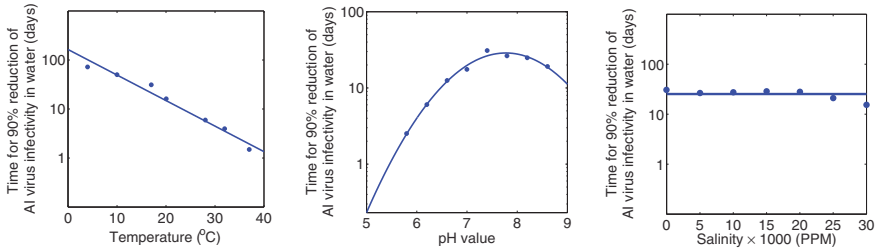

FIG. 2. *Best polynomial of the least degree fitted to the laboratory experimental data regarding time required for infectivity of AIV to be reduced by* 90% (a) *at different temperatures with pH value and salinity fixed at* 7.2 *and* 0 *ppm, respectively;* (b) *at different pH values with temperature and salinity fixed at* $17^\circ C$ *and* 0 *ppm, respectively; and* (c) *at different salinities with temperature and pH value fixed at* $17^\circ C$ *and* 7.2*, respectively. Note that the y-axis is on a log scale. Shown here is our own visualization of data from Brown et al.* [11]. *Parameter values are* $a_T = -0.12$, $b_T = 5.10$, $a_A = -0.63$, $b_A = 9.75$, $c_A = -34.53$, $a_\zeta = 3.21$.

data to obtain T_0, ϵ, and ϕ. This temperature function is then used as a known function while fitting influenza prevalence data as described in the sections to follow.

4.2. Parameter estimation and model selection. We take $\lambda = 2$, $k = 3.33 \times 10^{-4}$ bird^{-1}, and $d = 0.1$ year^{-1} [6, 8]. Since infected birds remain infectious for about one week (range 6–10 days) [9, 36, 43, 67], we consider the recovery rate, $\gamma = 1/7 \sim 0.14$ day^{-1}. The viral shedding rate, p, has been detected in experimental settings from $\sim 10^{0.5}$ EID_{50} [63] to $\sim 10^7$ EID_{50} [66], where EID_{50} denotes 50% egg infectious dose. We consider a shedding rate of $p = 10^3$ EID_{50} per infected bird per day for our base case computation and provide a sensitivity analysis of estimated parameters on the choice of p. Note that the choice of units of p, and hence V, are arbitrary for our purposes, as they ultimately scale out when computing prevalence. We take $V_0 = 10^{4.7}$ EID_{50} consistent with the minimal viral load ($\sim 10^{4.7}$ EID_{50}) recorded to initiate an infection with a LPAI virus [41]. Furthermore, we consider 10,000 initial susceptible birds, i.e., $S_0 = 10,000$, and $R_0 = 0$ for our base case computation. We also carry out an analysis of the sensitivity of any estimated parameters to these choices of V_0 and S_0. Parameters and their values are listed in Table 1.

We estimate four parameters, β_d, β_i, η, and $P_0 = I_0/(S_0 + I_0 + R_0)$, from field survey data in Northern Europe [43]. We solve the system of ODEs numerically using a fourth order Runge–Kutta integration and use the solutions to obtain the best-fit parameters via a nonlinear least squares regression method that minimizes the sum of the squared residuals. To obtain confidence limits for the estimated parameters, we compute standard deviations from the sensitivity matrix [4, 25, 34].

We perform statistical tests to evaluate the statistical significance of the fits obtained with different models: the original model with time-varying temperature, a simpler (existing) model with a constant decay rate, a model with direct transmission only, a model with indirect transmission only, and models with/without immunity loss. These statistical tests are presented in the appropriate subsections that follow. We perform F tests if the models are nested; otherwise we compare the small-sample (second order) Akaike information criterion (AIC_c) values.

4.3. The model fit to field data from Northern Europe. We obtained published AIV prevalence data from a large-scale study (about 5,000 birds) conducted in migratory waterfowl (mostly mallards) at Ottenby Bird Observatory, in southeast

TABLE 1
Parameters of the model

Symbol	Description	Value [SD]	Unit	Reference
		Demographic parameters		
λ	Fecundity	2	-	[8]
k	Survival rate	3.33×10^{-4}	bird^{-1}	[8]
d	Natural death rate	0.1 (0.05 – 0.3)	year^{-1}	[6, 8]
		Disease-related parameters		
β_d	Direct transmission rate	2.14×10^{-9} $[4.26 \times 10^{-9}]$	$\text{bird}^{-1}\ \text{day}^{-1}$	Data fitting
β_i	Indirect transmission rate	3.55×10^{-9} $[8.46 \times 10^{-10}]$	$\text{EID}_{50}^{-1}\ \text{day}^{-1}$	Data fitting
η	Immunity loss rate	0.038 $[7.17 \times 10^{-4}]$	day^{-1}	Data fitting
γ	Recovery rate	0.14	day^{-1}	[41, 66, 67]
p	Viral shedding rate	1×10^3	$\text{EID}_{50}\text{bird}^{-1}\text{day}^{-1}$	[49]

Sweden [64]. We considered the monthly average (year 2002–2005) influenza A prevalence in mallards from May to November as for these months the data for at least 3 of 4 years (2002, 2003, 2004, 2005) were collected (Figure 4 in Wallensten et al. [64]). These birds were found near Helsinki, Finland, during the summer months and Hamburg, Germany, during the winter months (Figure 1 in Wallensten et al. [64]). Therefore, we used time-dependent temperature profiles of Helsinki [19] and Hamburg [27] to represent breeding ground and wintering ground temperatures, respectively (Figure 3).

We note that only air temperature data is available, and the viral persistence in our model is related to water temperature in aquatic environments such as streams and ponds. In general, air temperatures and water temperatures, for example, in streams, have strong relationships [57], and daily analysis over a 1-year period [58] shows that the seasonal variability of atmospheric conditions influences air and stream water temperature fluctuations nearly proportionally. For temperatures averaged monthly, a regression line representing stream water temperature as a function of measured air temperature has slope $\sim$1 and intercept $\sim$1 [47], supporting the assumption that for monthly averaged temperatures, air temperature provides a good approximation to water temperature.

We fitted our model to the data to estimate the infection rates β_d and β_i, the rate at which immunity wanes, η, and the initial prevalence, P_0; all remaining parameters were fixed to values obtained from the literature (see Table 1). As seen in Figure 3, the model including time-varying temperature effects fits this Northern European dataset well. While the goodness of fit observed here is not surprising, given the small dataset, the best-fit values of parameters obtained in this fitting procedure give some insight into the components contributing to endemic AI dynamics. For example, the value of η, the immunity loss rate, obtained here is substantially higher than expected, based on previous estimates. We explain these surprising results further in the following sections and in the discussion. We also note that including a frequency-dependent direct infection term did not improve the model fit ($\text{AIC}_c = -27.86$ for mass action and -26.31 for frequency-dependent terms, respectively).

To understand the importance of including time-varying temperatures in fitting this dataset, we also performed data fitting using a model with a constant viral decay rate, $\Omega(E(t)) = \bar{\Omega}$. We note that in our full model, the viral decay rates at each temperature and the environmental temperature are known parameters. In contrast,

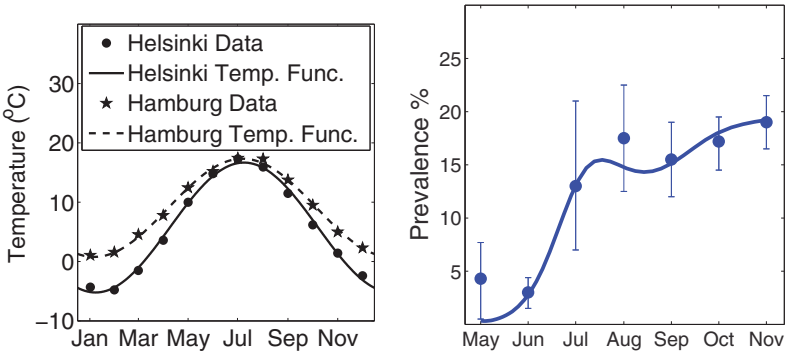

FIG. 3. (a) *Mean temperature profile for Helsinki, Finland (the breeding ground), and Hamburg, Germany (the wintering ground). Solid and dashed curves represent the time-varying temperature function* $T(t) = T_0(1 + \epsilon \sin(\omega t + \phi))$ *fitted to the data with* $\omega = 2\pi/365$. *For Helsinki,* $T_0 = 5.73$, $\epsilon = 1.91$, $\phi = 92.30$. *For Hamburg,* $T_0 = 9.05$, $\epsilon = 0.91$, $\phi = 92.23$. (b) *AI prevalence (%) predicted by the model (solid line) along with the data from a field survey in Northern Europe (filled circles). Parameters are given in Table* 1. *Shown here is our own visualization of data from Wallensten et al.* [64], *with bars indicating the standard error.*

$\bar{\Omega}$ is unknown, and thus the constant decay rate model requires estimates of one more parameter. To reduce the number of unknowns, we set $\beta_d = 0$ in both models, since the contribution from direct transmission for this dataset appears to be negligible (see section 5). Comparing the two models against the Ottenby dataset, we find that the model with time-varying temperature offers a statistically better fit ($\text{AIC}_c = -27.86$ for our full model and 17.05 for the constant decay rate model).

4.4. Temperature sensitivity. Using the parameter values thus estimated for the Ottenby dataset (Table 1), we explored the magnitude of the temperature sensitivity of each of the epidemiological measures derived analytically in section 3.

4.4.1. The basic reproductive number. The dependence of the reproductive number on temperature and pH is shown in Figure 4, which indicates a threshold average temperature of 24°C and threshold pH of 6.4. This predicts, for example, that AIV cannot spread in an environment in which the water temperature remains approximately constant with a value greater than 24°C. As seen in Figure 4, we estimate a reasonably large value of the basic reproductive number, $\mathcal{R}_0 = 5.3$, for Helsinki in May, the initial month considered in the dataset.

4.4.2. Final outbreak size. Using result (3.3), we likewise studied the effects of temperature on the final outbreak size, by computing the roots of $\mathcal{G}(\mathcal{Z})$ numerically. The final outbreak size is sensitive to temperature; the higher the temperature, the smaller the outbreak. For example, at a temperature of 20°C, the final outbreak size is just over 60%, but this approaches 100% for temperatures around 0°C.

4.4.3. The effective reproductive number. In Figure 5, we explore the effects of periodic temperature profiles on $\mathcal{R}_e(t)$, assuming sinusoidal temperature variations with a period of 1 year. We observe that at the parameter values for Northern Europe, the effective reproductive number is significantly affected by both the mean value and the amplitude of the periodic temperature profile. We note that $\mathcal{R}_e(t)$ is large at the beginning and the end of the breeding season, when temperatures are cooler, whereas during midsummer the value of $\mathcal{R}_e(t)$ is substantially reduced. This pattern is particularly interesting given the double peaks in AI prevalence which are

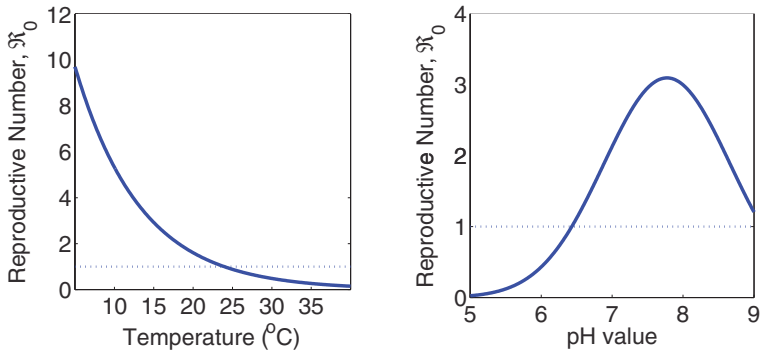

FIG. 4. *The basic reproductive number, $\mathcal{R}_0$, versus temperature and pH value with parameters for Northern Europe (Table 1).*

observed in spring and fall in field data. We also note that higher variability in temperature reduces $\mathcal{R}_e(t)$ in general.

4.4.4. AI invasion threshold. Using the results of section 3.4, we can compute $\mathcal{R}_i$ by solving $\rho(\mathcal{T}(\tau, \vartheta)) = 1$ numerically. This allows for an estimation of the sensitivity of the AI invasion threshold, $\mathcal{R}_i$, to the temperature profile (Figure 5). Our results show that $\mathcal{R}_i$ decreases as the mean temperature, T_0, increases, or as the amplitude of the periodic temperature profile increases. Therefore, AI has a higher chance of invading susceptible populations in an environment with a lower mean temperature or with reduced temperature fluctuations.

5. Epidemiological implications.

5.1. Direct versus indirect transmission. To compare the impact of direct and indirect transmission, we numerically computed the number of new infections generated via each route, during a 6-month period, using the best-fit parameters obtained for the Ottenby data. This analysis reveals that the number of new infections by direct transmission is four orders of magnitude smaller than the number by indirect transmission. We therefore explored data fitting in a reduced model in which direct transmission was neglected, i.e., $\beta_d = 0$; this resulted in only a slight change in the remaining estimated parameters (less than 5% in all cases). This reduced model fits the data equally well as compared to the full model (F test, $p > 0.05$). In contrast, if we include direct transmission but neglect indirect transmission ($\beta_i = 0$), the model fit is significantly worse than the full model (F test, $p = 0.0183$). These results are consistent with the suggestion that the transmission of AI among wild birds is largely through the indirect fecal-oral route [11, 32, 33, 66], underscoring the need for models which explicitly include the effects of water temperature on viral persistence. Given the limited data points from Ottenby, however, we cannot rule out the possibility that direct transmission is the dominant route in other parameter ranges. We therefore allowed β_d to be nonzero in the sensitivity analyses and other explorations of parameter space. In fact, using the basic reproductive number and assuming a constant viral decay rate $\bar{\Omega}$, we can obtain a threshold expression, $\bar{\Omega}^* = \beta_i p/\beta_d$, such that if $\bar{\Omega} < \bar{\Omega}^*$ ($\bar{\Omega} > \bar{\Omega}^*$) direct (indirect) transmission dominates.

5.2. Short duration of acquired immunity. The immune response against AIV in wild birds is poorly understood, yet the parameter η, which represents the reciprocal of the mean duration of immunity acquired due to AIV infection, plays an important role in the disease dynamics. In previous studies, this parameter was

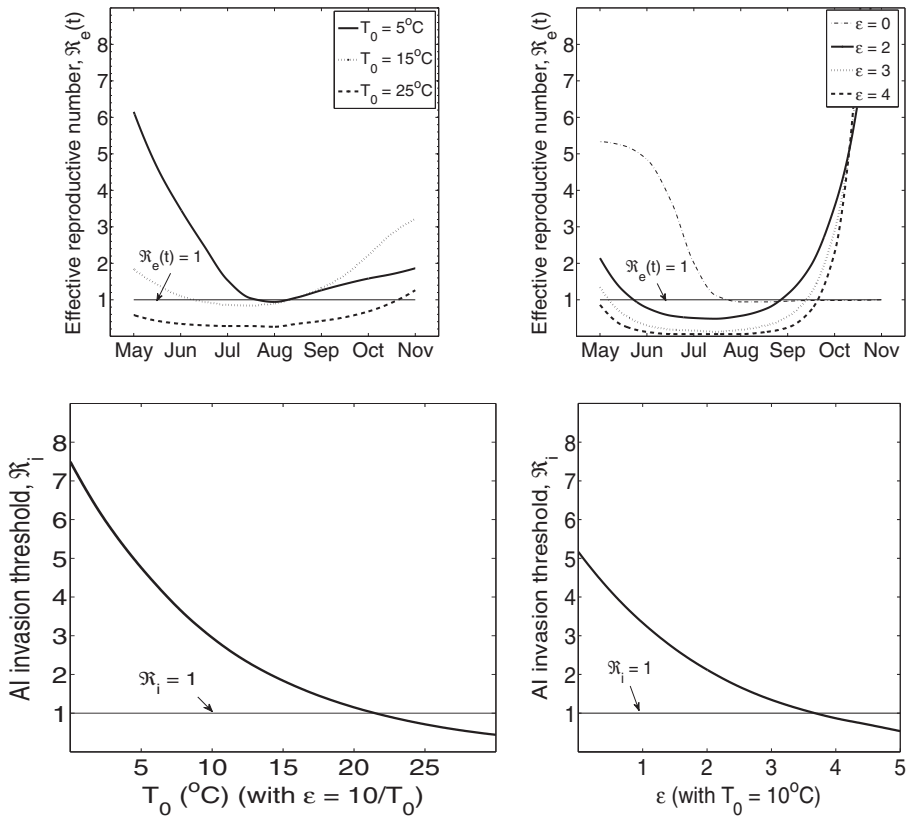

FIG. 5. *The effective reproductive number versus time ($\mathcal{R}_e(t)$, top panels), and the AI invasion threshold ($\mathcal{R}_i$, bottom panels), for values of T_0 with ϵ fixed at $10/T_0$ (left panels) and ϵ with T_0 fixed at $10°C$ (right panels).*

not considered, assuming permanent immunity [8, 31], or taken to correspond to an immune period of more than a year [49]. However, our model predicts that birds infected by AIV lose their immunity in approximately 4 weeks, significantly shorter than values used previously. If we consider the Ottenby dataset used in this study, 15%–20% AIV prevalence was maintained for more than 4 months each summer. Since infected birds recover from AI in about a week, if they have permanent immunity, infection of the entire bird population takes only 5 weeks. Hence, to maintain 15%–20% prevalence for several months as seen in the dataset, the birds need to lose immunity in about 4 weeks. This rough calculation yields an immunity loss rate of $1/28 = 0.036$ per day, which is consistent with our estimate of $\eta = 0.038$ per day. We find that lifetime immunity cannot explain this dataset. To confirm this we fitted the data using a model that ignores the term representing immunity loss (i.e., $\eta = 0$); this yielded a significantly worse fit to the data (F test, $p < 0.001$).

5.3. Environmental effects on single-season dynamics. We used the OSOG model to study the effects of temperature on influenza prevalence during a single season. Even within a single season, the temperature varies widely. Moreover, the temperature profile varies from location to location as well as year to year. To demonstrate how this variation affects disease dynamics, we considered two different locations—Helsinki, Finland (the breeding ground for the Ottenby data), and

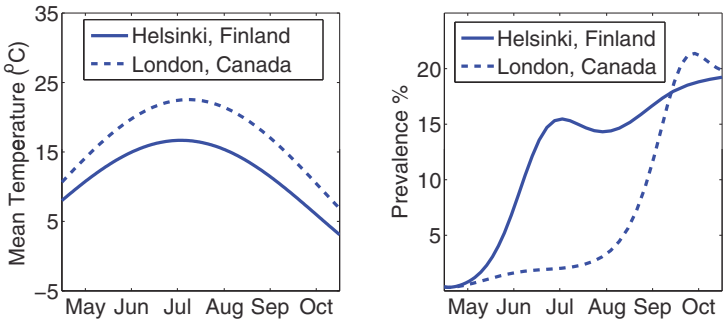

FIG. 6. (a) *The breeding season time-varying temperature function* $T(t) = T_0(1+\epsilon \sin(\omega t + \phi))$ *obtained by fitting to monthly average temperature data from Helsinki, Finland, and London, Ontario, with a* 1*-year period. For London,* $T_0 = 8.98$, $\epsilon = 1.54$, $\phi = 60.98$ *(see Figure* 3 *for Helsinki).* (b) *AI prevalence (%) within a single breeding season for these two temperature profiles. All other parameters are as in Table* 1 *for both locations.*

London, Ontario—both of which support wild waterfowl populations in summer. Using our model, we predicted the influenza prevalence using climate data from Helsinki [19] and London [17], respectively, while keeping all other disease parameters the same for both locations. Although the difference in temperatures between the two locations remains less than 8°C at each time point (Figure 6(a)), the predicted dynamics of influenza prevalence are quite different in these locations (Figure 6(b)). For example, in the month of July, the mean temperature in Helsinki is only 5.7°C less than London, yet our model predicts the influenza prevalence among London birds is more than 70% less than that among Helsinki birds. Note that Helsinki has a lower mean level ($T_0 = 5.73$) and a lower amplitude ($\epsilon T_0 = 10.9$) in the temperature profile than London ($T_0 = 8.98, \epsilon T_0 = 13.8$), indicating a longer persistence of the virus in Helsinki. This results in a quick rise of prevalence in Helsinki, peaking in early summer, while the prevalence in London remains low for several months longer, rising to a peak level in the fall. This shows that temperature changes can significantly impact disease dynamics even within a single season, again underlining the importance of considering time-varying temperature profiles for accurate prediction of AI dynamics.

5.4. Environmental effects on long-term dynamics. To understand the long-term disease dynamics, we used the TSTG model, integrating the equations numerically for sufficiently long that the system stabilizes to a repeated annual cycle. We again use the parameter ϵ of the temperature function $T(t) = T_0(1+\epsilon \sin(\omega t + \phi))$ to study the effect of time-varying temperatures on the long-term disease dynamics. Figure 7 shows a 1-year time series (in the long term) of influenza prevalence among wild birds for different values of ϵ. Here $\epsilon = 0$ yields a constant temperature, i.e., a model which is equivalent to previous models with constant viral decay rates; higher values of ϵ give temperature profiles of larger amplitude. Temperature variations over time clearly impact long-term influenza prevalence in wild birds; in particular greater variation produces larger fluctuations in influenza prevalence throughout the year. Interestingly, seasonal variations in temperature can generate double peaks in AI prevalence, as observed in real data [43]; these double peaks do not occur when $\epsilon = 0$. A larger variation in temperature results in a deeper well between these double peaks.

5.5. Sensitivity to fixed parameters. In our data fitting process, the parameters p (shedding rate), S_0 (initial susceptible bird population), and V_0 (initial

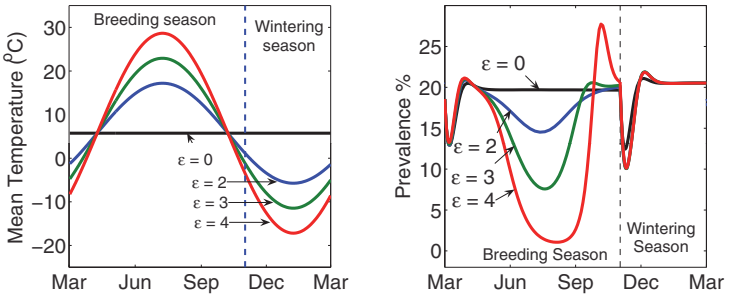

FIG. 7. *Mean temperature profile for different ϵ and corresponding 1-year time series of AI prevalence (%) in wild birds in the long term. While the parameter ϵ is varied, all other parameters are fixed as in Table* 1.

viral concentration) were fixed. However, the values of these parameters may vary depending upon a number of factors. For example, experiments show that older birds shed viral RNA at higher rates than younger birds [63]. It is straightforward to show that the model system becomes independent of S_0 if the scalings $\beta_d \to \beta_d/S_0$ and $p \to p/S_0$ are performed; thus the sensitivity to S_0 can be obtained from the sensitivity to p and by scaling estimates of β_d. To address the sensitivity of our conclusions to p and V_0, we performed data fitting and model simulation for changes in V_0 from 3 $\log_{10}$ to 6 $\log_{10}$ EID_{50} and changes in p from 100 to 10,000 EID_{50} per bird per day. This sensitivity analysis revealed that the qualitative conclusions of this study are not affected by changes of several orders of magnitude in these parameters. In addition, we examined the sensitivity of two quantitative conclusions: that the period of immunity for infected birds is about 4 weeks and that the number of new infections generated by direct transmission is four orders of magnitude less than those generated by indirect transmission. Neither of these conclusions was affected by changes in these initial parameter estimates.

6. Discussion. Since aquatic wild birds represent both a natural reservoir for recombination of various AIV strains and a source of novel strains with potential pathogenicity in humans, the transmission dynamics of AIV in wild bird populations is of important scientific and public health interest. Previous mathematical models [5, 6, 7, 8, 31, 49, 50] have offered valuable insights into AI dynamics among wild birds, highlighting the importance of indirect fecal-oral transmission and seasonal bird migration. Recent evidence has demonstrated that environmental conditions directly impact the persistence of AIV in water [10, 11, 14, 55, 66], which has a significant contribution to fecal-oral transmission. In particular, laboratory experiments have shown that a change in the environment over time—even within a few weeks—can result in substantial variation in viral persistence [11].

Here, we developed mathematical models taking time-varying environmental factors, particularly time-varying temperature, into account. We analyzed the model to study how environmental temperature affects the basic reproductive number, $\mathcal{R}_0$, the effective reproductive number, $\mathcal{R}_e(t)$, and the AI invasion threshold, $\mathcal{R}_i$. We also analyzed the global dynamics predicted by a periodic environmental temperature and derived a condition for long-term AI persistence in wild birds. We find that the relative contribution of direct versus indirect transmission to the basic reproductive number, $\mathcal{R}_0$, can differ substantially depending upon environmental conditions such

as temperature and pH; in particular, the contribution of indirect transmission, $\mathcal{R}_0^i$, varies according to these environmental conditions. For example, as the environment gets cooler, $\mathcal{R}_0^i$ becomes larger (Figure 4). We derive a threshold formula which predicts whether direct or indirect transmission is dominant. These theoretical results underscore the importance of indirect transmission since the critical value ($\mathcal{R}_0 > 1$) can be achieved—and the pathogen may persist—due to environmental variations, even when the direct transmission of AIV among wild birds is low ($\mathcal{R}_0^d < 1$). For Northern Europe, we predict that $\mathcal{R}_0 > 1$ resulting in endemic disease for average monthly temperatures below 24°C and pH above 6.4. We also find that in a model for a short-term AI epidemic with $\mathcal{R}_0 > 1$ (i.e., an OSOG model with $d = \eta = 0$), the disease eventually dies out (Lemma 3.1), resulting in a temperature-dependent final outbreak size; a higher environmental temperature gives a lower final outbreak size.

Our results show that environmental temperatures also play a significant role in determining the effective reproductive number as well as the AI invasion threshold and AI persistence in wild birds. The effective reproductive number is highly sensitive to both the mean and the amplitude of the periodic temperature profile (Figure 5). Moreover, as demonstrated by our formulation of the AI invasion threshold, global climate change may have substantial implications for the prevalence of AI among wild birds (Figure 5); higher and more variable temperatures pose more obstacles to AI invasion as well as long-term AI persistence in wild birds.

In numerical work, we verified that the model provides an excellent fit to AIV prevalence data from a field survey in Northern Europe (Figure 3) and in fact gives a statistically better fit to the data compared to the same model with a constant environmental viral decay rate. While we acknowledge that the data are limited, the parameters estimated for Northern Europe provide some interesting insight into disease characteristics. First, our results are consistent with previous suggestions that the primary route of AI transmission among these wild birds is via the indirect fecal-oral route [11, 32, 33, 66]. Our estimates further suggest that infected birds lose immunity against AIV in about 4 weeks, which is substantially shorter than previously considered [8, 31, 49]. The rapid waning of immunity estimated in this study is also supported by an experimental study [51] which examined immunity against influenza in a group of chickens infected by the LPAI virus sub-type H9N2, even though the mechanism of immunity in chickens and wild birds may not be the same. This prediction has important biological implications: a short period of immunity suggests that long-lived memory cells are not generated by this infection. If this is the case, vaccination with LPAI viruses might not be a good strategy for long-term disease control. However, we note that the mechanism and dynamics of natural and artificial immunity can be different, and exposure to LPAI has been seen to provide some protection against highly pathogenic avian influenza for longer than 4 weeks in other studies [20, 21]. An alternate explanation for this rapidly waning immunity could be that the virus mutates rapidly, producing multiple strains which are capable of immune escape in previously infected and recovered birds. More data considering multiple strains and immune responses are necessary to clarify this issue.

Our single-season simulations for temperatures recorded in Helsinki, Finland, show that the maximum prevalence in Helsinki occurs in the months of October and November (just before fall migration) (Figure 6(b)) when the temperature reaches about 0°C (Figure 6(a)). This is consistent with a study by Reperant et al. [48] in which outbreaks of H5N1 influenza in waterbirds were clustered along the 0°C isotherm in Europe during the winter of 2005–2006. Moreover, our results for temperature profiles in Helsinki, Finland, and London, Canada, show that even moder-

ately different temperature profiles can produce substantially different dynamics of AIV prevalence (for example, prevalence differs by over 70% in July, despite <8°C difference in temperature at each time point in Figure 6). Cooler places with lower temperature variation such as Helsinki provide an environment in which the virus persists longer, causing a rapid rise in prevalence.

Using the TSTG model we also studied the effects of different time-varying temperature profiles on long-term AI dynamics. The time course of annual AI prevalence is strongly affected by time-varying temperature profiles (Figure 7). This sensitivity is more pronounced during the breeding season than the wintering season. More importantly, variations in temperature over time can produce double-peak prevalence profiles, as observed in real data [43]. The larger the temperature variation over time, the deeper the well between these two peaks. We also find (data not shown) that interannual variations in temperature produce corresponding interannual variations in AI dynamics. Since only 3 years of data are available in the Ottenby dataset, this remains an intriguing avenue for future work, as more data become available. The result suggests, however, that year-to-year temperature variation may be an additional cause of interannual stochasticity in AI dynamics; previous approaches have used stochastic terms to capture these effects [8].

There are several limitations of this study. Our data fitting is based on limited AI prevalence data, lending uncertainty to the parameters estimated. Seasonal data from other locations, where environmental conditions differ, will be necessary to better understand the effects of place-to-place environmental variation on AI dynamics. We used a deterministic approach to analyze time-varying environmental effects but acknowledge that stochastic effects might also have an impact. Finally, our assumption of instantaneous migration may be less realistic for birds such as bar-headed geese which use many stopover locations during migration [6, 28]. However, once data for stopover sites are known, our model could easily be extended by considering one or more stopover grounds apart from the breeding and wintering grounds.

Appendix A. Proof of Lemma 3.5. First we note that the linearized system (3.4)–(3.5) preserves positivity and therefore from (3.4) we can write $dI/dt \geq (\beta_d S_0 - \gamma - d)I$. This implies that if $\mathcal{R}_0^d > 1$, i.e., $(\beta_d S_0 - \gamma - d) > 0$, then $I \to \infty$ as $t \to \infty$, i.e., the disease-free equilibrium is unstable for any $\Omega(t)$. Thus, we assume that $\mathcal{R}_0^d < 1$. As discussed in [28, 70], the Floquet multiplier theory and the Perron–Frobenius theory combined imply that there exist positive τ-periodic functions $(\bar{I}(t), \bar{V}(t))^T$ such that $(I(t), V(t))^T = e^{\Theta t}(\bar{I}(t), \bar{V}(t))^T$ is a solution of system (3.4)–(3.5), where $e^{\Theta\tau}$ represents the spectral radius of the matrix $\Phi_{\mathcal{F}_\tau - \mathcal{V}_\tau}(\tau)$. Note that it is sufficient to consider only real values of Θ. Then, $(\bar{I}(t), \bar{V}(t))^T$ satisfy

$$\frac{d\bar{I}}{dt} = (\beta_d S_0 - \gamma - d - \Theta)\bar{I} + \beta_i S_0 \bar{V},$$
$$\frac{d\bar{V}}{dt} = p\bar{I} - (\Omega(t) + \Theta)\bar{V}.$$

These differential equations have solutions

$$\bar{V}(t) = p \int_{-\infty}^{t} \bar{I}(s) \exp\left(- \int_s^t (\Omega(\bar{s}) + \Theta) d\bar{s} \right) ds,$$
$$\bar{I}(t) = \beta_i S_0 \int_{-\infty}^{t} e^{-(\gamma + d - \beta_d S_0 + \Theta)(t-s)} \bar{V}(s) ds,$$

which can be combined to yield the integral equation

$$\bar{I}(t) = p\beta_i S_0 \int_{-\infty}^{t} e^{-(\gamma+d-\beta_d S_0+\Theta)(t-s)} \int_{-\infty}^{s} \bar{I}(\bar{s})\exp\left(-\int_{\bar{s}}^{s}(\Omega(\bar{\bar{s}})+\Theta)d\bar{\bar{s}}\right) d\bar{s}ds.$$

Since $\bar{I}(t)$ is periodic, it has a maximum, and

$$\bar{I}(t)\leq\left[\max_{\xi\in[0,\tau]}\bar{I}(\xi)\right] p\beta_i S_0\int_{-\infty}^{t} e^{-(\gamma+d-\beta_d S_0+\Theta)(t-s)}\int_{-\infty}^{s}\exp\left(-\int_{\bar{s}}^{s}(\Omega(\bar{\bar{s}})+\Theta)d\bar{\bar{s}}\right) d\bar{s}ds.$$

We claim that $\Theta < 0$ if $Q(t) < 1\ \forall t \in \mathbb{R}$. Otherwise, if $\Theta \geq 0$, then from the above it follows that

$$\bar{I}(t) \leq \left[\max_{\xi\in[0,\tau]}\bar{I}(\xi)\right] Q(t).$$

Now, let $t^* \in [0,\tau]$ be such that $\bar{I}(t^*) = \max_{\xi\in[0,\tau]}\bar{I}(\xi)$. This implies $Q(t^*) \geq 1$, which contradicts the hypothesis that $Q(t) < 1\ \forall t \in \mathbb{R}$. Thus if $Q(t) < 1\ \forall t \in \mathbb{R}$, then $\Theta < 0$ and $(I(t), V(t)) \to (0,0)$ as $t \to \infty$.

Appendix B. Proof of Theorem 3.6. For any $(S_0, I_0, N_0, V_0) \in \mathbb{R}^4_+$, system (3.7)–(3.10) has a unique local non-negative solution $(S(t), I(t), N(t), V(t))$ through the initial value $(S(0), I(0), N(0), V(0)) = (S_0, I_0, N_0, V_0)$ [53]. From (3.9), the unique equilibrium $N^* = \Lambda/d$ is globally asymptotically stable, and $N(t)$ is ultimately bounded. Also, $dV/dt = pI - \Omega(t)V \leq pN - \Omega_m V$, where $\Omega_m = \Omega(T_{\min})$, and $T_{\min}$ is assumed to represent a realistic minimum temperature under which wild birds can survive. Again, $dV/dt = pN - \Omega_m V$ provides a limiting system $dV/dt = p\Lambda/d - \Omega_m V$, which has a globally asymptotically stable unique equilibrium $V^* = \Lambda p/(\Omega_m d)$. Then, by the comparison principle [54], $V(t)$ is also ultimately bounded. Hence, the solutions of the system (3.7)–(3.10) exist globally on the interval $[0,\infty)$. In summary, we have the following theorem.

THEOREM B.1. *System* (3.7)–(3.10) *has a unique and bounded solution with the initial value* $(S_0, I_0, N_0, V_0) \in \mathbb{D} := \{(S, I, N, V) \in \mathbb{R}^4_+ : S + I \leq N\}$. *Furthermore, for any* $q > 0$, *there exists* $t_q > 0$ *such that the solution of system* (3.7)–(3.10) *with* $t \geq t_q$ *lies in the compact set* $\mathbb{D}_{\Omega+q} = \{(S, I, N, V) \in \mathbb{D} : N \leq \Lambda/d + q, V \leq \Lambda p/(\Omega_m d) + q\}$.

Let $\mathcal{R}_i < 1$. Then Lemma 3.4 implies that X_0 is locally asymptotically stable, i.e., $\rho\left(\Phi_{\mathcal{F}_\tau - \mathcal{V}_\tau}(\tau)\right) < 1$. We can choose $q_0 > 0$ small enough giving $\rho\left(\Phi_{\mathcal{F}_\tau - \mathcal{V}_\tau + \mathcal{M}_{q0}}(\tau)\right) < 1$, where

$$\mathcal{M}_{q0} = \begin{pmatrix} \beta_d q_0 & \beta_i q_0 \\ 0 & 0 \end{pmatrix}.$$

From (3.9), $N(t) \to \Lambda/d$ as $t \to +\infty$. Therefore, for $q_0 > 0$, there exists $t_{q0} > 0$ such that $S(t) \leq N(t) \leq \Lambda/d + q_0\ \forall t \geq t_{q0}$. Then from system (3.7)–(3.10), we have

$$dI/dt \leq \left(\frac{\beta_d\Lambda}{d} - \gamma - d + \beta_d q_0\right) I + \left(\frac{\beta_i\Lambda}{d} + \beta_i q_0\right) V, \tag{B.1}$$

$$dV/dt = pI - \Omega(t)V. \tag{B.2}$$

Now, consider the following comparison system:

$$\begin{pmatrix} d\hat{I}/dt \\ d\hat{V}/dt \end{pmatrix} = (\mathcal{F}_\tau - \mathcal{V}_\tau + \mathcal{M}_{q0}) \begin{pmatrix} \hat{I} \\ \hat{V} \end{pmatrix}. \tag{B.3}$$

According to Zhang and Zhao [70], there exists a positive, τ-periodic function $(\bar{I}(t), \bar{V}(t))^T$ such that $(\hat{I}(t), \hat{V}(t))^T = e^{\Theta t}(\bar{I}(t), \bar{V}(t))^T$ is a solution of system (B.3), where $\Theta = \ln \rho(\Phi_{\mathcal{F}_\tau - \mathcal{V}_\tau + \mathcal{M}_{q0}}(\tau))/\tau$. Here, $\rho\left(\Phi_{\mathcal{F}_\tau - \mathcal{V}_\tau + \mathcal{M}_{q0}}(\tau)\right) < 1 \Rightarrow \Theta < 0$, which implies $(\hat{I}(t), \hat{V}(t))^T \to (0,0)^T$ as $t \to +\infty$. Therefore, the $(0,0)^T$ solution of system (B.3) is globally asymptotically stable.

For any nonnegative initial value $(I(0), V(0))^T$ of system (B.1)–(B.2), we can choose a sufficiently large $m > 0$ satisfying $(I(0), V(0))^T \le m(\bar{I}(0), \bar{V}(0))^T$. Clearly, $m(\hat{I}(t), \hat{V}(t))^T = me^{\Theta t}(\bar{I}(t), \bar{V}(t))^T$ is also a solution of (B.3). Then applying the comparison principle [54], we get $(I(t), V(t))^T \le m(\hat{I}(t), \hat{V}(t))^T \ \forall t > 0$. Therefore, we get $I(t) \to 0$, and $V(t) \to 0$ as $t \to +\infty$. Then, by the theory of asymptotic autonomous systems [60], we get $S(t) \to \Lambda/d, N(t) \to \Lambda/d$ as $t \to +\infty$. Hence, $\mathcal{R}_i < 1$ gives a condition for X_0 to be globally asymptotically stable.

Appendix C. Proof of Theorem 3.7. Consider

$$\mathbb{D}_0 := \{(S, I, N, V) \in \mathbb{D} : I > 0, V > 0\} \quad \text{and} \quad \partial\mathbb{D}_0 := \mathbb{D} \backslash \mathbb{D}_0.$$

Define the Poincaré map $P : \mathbb{D} \to \mathbb{D}$ associated with system (3.7)–(3.10) by $P(z_0) = u(\tau, z_0) \ \forall z_0 \in \mathbb{D}$, where $u(t, z_0)$ is the unique solution of system (3.7)–(3.10) with $u(0, z_0) = z_0 = (S_0, I_0, N_0, V_0)$. Then $P^n(z_0) = u(n\tau, z_0) \ \forall n \ge 0$.

Let $\mathcal{R}_i > 1$. In this case, the disease-free equilibrium $X_0 = (\Lambda/d, 0, \Lambda/d, 0)$ is an isolated invariant set in $\mathbb{D}$, and $W^s(X_0) \cap \mathbb{D}_0 = \phi$, where $W^s(X_0)$ is the stable set of X_0, as stated in the following lemma.

LEMMA C.1. *If $\mathcal{R}_i > 1$, then there exists a $\sigma^* > 0$ such that for any $z_0 = (S_0, I_0, N_0, V_0) \in \mathbb{D}_0$ with $||z_0 - X_0|| \le \sigma^*$, we have*

$$\limsup_{n\to\infty} \mathrm{D}(P^n(z_0), X_0) \ge \sigma^*,$$

where $\mathrm{D}(Z, X)$ denotes the distance between Z and X in $\mathbb{R}^4$.

Proof. Since $\mathcal{R}_i > 1$, Lemma 3.4 implies that X_0 is unstable, i.e., $\rho\left(\Phi_{\mathcal{F}_\tau - \mathcal{V}_\tau}(\tau)\right) > 1$. We can choose $q_1 > 0$ small enough giving $\rho\left(\Phi_{\mathcal{F}_\tau - \mathcal{V}_\tau - \mathcal{M}_{q1}}(\tau)\right) > 1$, where

$$\mathcal{M}_{q1} = \begin{pmatrix} \beta_d q_1 & \beta_i q_1 \\ 0 & 0 \end{pmatrix}.$$

Note that the equation $dS/dt = \Lambda - dS$ has a unique equilibrium $S^* = \Lambda/d$, which is globally attractive in $\mathbb{R}_+$. Also, the perturbed system

$$d\hat{S}(t)/dt = \Lambda - d\hat{S}(t) - (\sigma\beta_d + \sigma\beta_i)\hat{S}(t) \tag{C.1}$$

has a unique equilibrium $\hat{S}^* = \Lambda/(\sigma\beta_d + \sigma\beta_i + d)$, which is globally attractive in $\mathbb{R}_+$. Since $\hat{S}^*$ is a continuous function of σ with $\lim_{\sigma\to 0} \hat{S}^* = \Lambda/d$, we can find sufficiently small σ_1 such that $\hat{S}^* > \Lambda/d - q_1 \ \forall \sigma \le \sigma_1$.

By the continuity of the solutions with respect to the initial values, there exists a $\sigma^* > 0$ such that any $z_0 \in \mathbb{D}_0$ with $||z_0 - X_0|| \le \sigma^*$ implies $||u(t, z_0) - u(t, X0)|| < \sigma_1 \ \forall t \in [0, \tau]$. We now prove that

$$\limsup_{n\to\infty} \mathrm{D}(P^n(z_0), X_0) \ge \sigma^*.$$

If possible suppose that the limit above $< \sigma^*$ for some $z_0 \in \mathbb{D}_0$. Without loss of generality we assume that $\mathrm{D}(P^n(z_0), X_0) < \sigma^* \ \forall n \ge 0$. This implies, by continuity, that

$$||u(t, P^n(z_0)) - u(t, X_0)|| < \sigma_1 \ \forall n \ge 0, \forall t \in [0, \tau].$$

Note that any $t \geq 0$ can be expressed as $t = n\tau + \tilde{t}$ with $\tilde{t} \in [0, \tau)$ and n, the largest integer less than or equal to t/τ. Therefore,

$$||u(t, z_0) - u(t, X_0)|| = ||u(\tilde{t}, P^n(z_0)) - u(\tilde{t}, X_0)|| < \sigma_1 \ \forall t \geq 0.$$

Substituting $u(t, z_0) = (S(t), I(t), N(t), V(t))$ and $u(t, X_0) = X_0$, we obtain $I(t) < \sigma_1$, $V(t) < \sigma_1$ $\forall t \geq 0$. Also, $(I(t) + S(t)) \leq N(t)$ $\forall t \geq 0$. Then, from (3.7), we obtain $dS/dt \geq \Lambda - (\beta_d \sigma_1 + \beta_i \sigma_1 + d)S$.

Take $\sigma = \sigma_1$. Then by the comparison, $S(t) \geq \hat{S}(t)$. Also, using $\lim_{t\to\infty} \hat{S}(t) = \hat{S}^* > \Lambda/d - q_1$, we obtain $S(t) \geq \Lambda/d - q_1$ for sufficiently large t. Using this in (3.8) and (3.10), we obtain, for sufficiently large t, that

$$dI/dt \geq \left(\frac{\beta_d \Lambda}{d} - \beta_d q_1 - \gamma - d\right) I + \left(\frac{\beta_i \Lambda}{d} - \beta_i q_1\right) V, \tag{C.2}$$

$$dV/dt = pI - \Omega(t)V. \tag{C.3}$$

Again, for a comparison system

$$\begin{pmatrix} d\hat{I}/dt \\ d\hat{V}/dt \end{pmatrix} = (\mathcal{F}_\tau - \mathcal{V}_\tau - \mathcal{M}_{q1}) \begin{pmatrix} \hat{I} \\ \hat{V} \end{pmatrix}, \tag{C.4}$$

there exists a positive, τ-periodic function $(\bar{I}(t), \bar{V}(t))^T$ such that $(\hat{I}(t), \hat{V}(t))^T = e^{\Theta_1 t}(\bar{I}(t), \bar{V}(t))^T$ is a solution of system (C.4), where $\Theta_1 = \ln \rho(\Phi_{\mathcal{F}_\tau - \mathcal{V}_\tau - \mathcal{M}_{q1}}(\tau))/\tau$ [70]. Here, $\rho\left(\Phi_{\mathcal{F}_\tau - \mathcal{V}_\tau - \mathcal{M}_{q1}}(\tau)\right) > 1 \Rightarrow \Theta_1 > 0$, which implies that, for nonnegative integer n, $(\hat{I}(n\tau), \hat{V}(n\tau))^T = e^{\Theta_1 n\tau}(\bar{I}(n\tau), \bar{V}(n\tau))^T \to (\infty, \infty)^T$ as $n \to \infty$.

For any nonnegative initial value $(I(0), V(0))^T$ of system (C.2)–(C.3), we can choose a sufficiently small $m_1 > 0$ satisfying $(I(0), V(0))^T \geq m_1(\bar{I}(0), \bar{V}(0))^T$. Clearly, $m_1(\hat{I}(t), \hat{V}(t))^T = m_1 e^{\Theta_1 t}(\bar{I}(t), \bar{V}(t))^T$ is also a solution of (C.4). Then applying the comparison principle [54], we get $(I(t), V(t))^T \geq m_1(\hat{I}(t), \hat{V}(t))^T$ $\forall t > 0$. Therefore, we get $I(n\tau) \to \infty$, and $V(n\tau) \to \infty$ as $n \to \infty$, which is a contradiction. This completes the proof. □

We know from Theorem B.1 that $\{P^n\}_{n\geq 0}$ admits a global attractor in $\mathbb{D}$. We now prove that $\{P^n\}_{n\geq 0}$ is uniformly persistent with respect to $(\mathbb{D}_0, \partial\mathbb{D}_0)$. For any $z_0 \in \mathbb{D}_0$, from (3.7), we have

$$S(t) = e^{-\int_0^t \eth(\tilde{s})d\tilde{s}} \left[S_0 + \left(\int_0^t e^{\int_0^{\tilde{s}_1} \eth(\tilde{s})d\tilde{s}} \Lambda_1(\tilde{s}_1) d\tilde{s}_1\right)\right], \tag{C.5}$$

where $\eth(t) = \beta_d I(t) + \beta_i V(t) + d + \eta > 0$ and $\Lambda_1(t) = \Lambda + \eta(N(t) - I(t)) > 0$. This implies $S(t) > 0$ $\forall t > 0$. As generalized to nonautonomous systems [53], the irreducibility of the cooperative matrix

$$\tilde{M}(t) = \begin{pmatrix} \beta_d S(t) - \gamma - d & \beta_i S(t) \\ p & -\Omega(t) \end{pmatrix}$$

implies that $(I(t), V(t))^T \gg 0$ $\forall t > 0$. Thus both $\mathbb{D}$ and $\mathbb{D}_0$ are positively invariant. Clearly, $\partial\mathbb{D}_0$ is relatively closed in $\mathbb{D}$.

Note that

$$M_\partial := \{z_0 \in \partial\mathbb{D}_0 : P^n(z_0) \in \partial\mathbb{D}_0 \ \forall n \geq 0\} = \{(S, 0, N, 0) \in \mathbb{D} : S \geq 0, N \geq 0\}, \tag{C.6}$$

i.e., for any $z_0 = (S_0, I_0, N_0, V_0) \in \{z_0 \in \partial\mathbb{D}_0 : P^n(z_0) \in \partial\mathbb{D}_0 \ \forall n \geq 0\}$, we have $I(n\tau) = V(n\tau) = 0 \ \forall n \geq 0$. If this is not true, then we can get some integer $n_1 \geq 0$ such that $(I(n_1\tau), V(n_1\tau))^T > 0$. Then by taking $n_1\tau$ as an initial time, (C.5) gives $S(t) > 0 \ \forall t > n_1\tau$. As mentioned above, generalization to nonautonomous systems provides $(I(t), V(t))^T \gg 0 \ \forall t > n_1\tau$, where the initial value $(I(n_1\tau), V(n_1\tau))^T > 0$. This gives $P^n(z_0) \in \mathbb{D}_0 \Rightarrow z_0 \notin \{z_0 \in \partial\mathbb{D}_0 : P^n(z_0) \in \partial\mathbb{D}_0 \ \forall n \geq 0\}$, a contradiction. Hence (C.6) is true.

Note that the disease-free equilibrium $X_0 = (\Lambda/d, 0, \Lambda/d, 0)$ is a unique fixed point of P in M_∂. Moreover, from Lemma C.1, X_0 is an isolated invariant set in $\mathbb{D}$, and $W^s(X_0) \bigcap \mathbb{D} = \phi$. Also, using $I = V = 0$ in system (3.7)–(3.10), the resulting linear nonhomogeneous system

$$\begin{aligned} dS/dt &= \Lambda - (\eta + d)S + \eta N, \\ dN/dt &= \Lambda - dN \end{aligned}$$

admits a global asymptotic stable equilibrium $(\Lambda/d, \Lambda/d)$. Note that every orbit in M_∂ approaches to X_0, and X_0 is acyclic in M_∂. By Zhao [71], it follows that $\{P^n\}_{n\geq 0}$ is uniformly persistent with respect to $(\mathbb{D}_0, \partial\mathbb{D}_0)$, and the solutions of system (3.7)–(3.10) are uniformly persistent with respect to $(\mathbb{D}_0, \partial\mathbb{D}_0)$, i.e., there exists a $\delta > 0$ such that any solution $(S(t), I(t), N(t), V(t))$ of system (3.7)–(3.10) with initial value $(S_0, I_0, N_0, V_0) \in \mathbb{D}_0$ satisfies $\liminf_{t\to\infty} I(t) \geq \delta$, and $\liminf_{t\to\infty} V(t) \geq \delta$.

Furthermore, P has a fixed point $(S^*(0), I^*(0), N^*(0), V^*(0)) \in \mathbb{D}_0$ [71]. Then $S^*(0) \geq 0, I^*(0) > 0, N^*(0) \geq 0$, and $V^*(0) > 0$. Also, $N(t) \geq S(t) + I(t) \ \forall t \geq 0$ implies that $N^*(0) > 0$. Moreover, there exists some $\bar{t} \in [0, \tau]$ with $S^*(\bar{t}) > 0$. If this is not true, we have $S^*(\bar{t}) \equiv 0 \ \forall t \in [0, \tau]$. Then, due to the periodicity of $S^*(t)$, we have $S^*(t) \equiv 0 \ \forall t \geq 0$. Then, from (3.7), $0 = \Lambda + \eta(N - I) > 0$, which is a contradiction. Thus we obtain

(C.7)
$$S^*(t) = e^{-\int_{\bar{t}}^{t} \eth^*(\tilde{s})d\tilde{s}} \left[S^*(\bar{t}) + \left(\int_{\bar{t}}^{t} e^{\int_{\bar{t}}^{\tilde{s}_1} \eth^*(\tilde{s})d\tilde{s}} \Lambda_1^*(\tilde{s}_1)d\tilde{s}_1 \right) \right] > 0 \ \forall t \in [\bar{t}, \bar{t} + \tau],$$

where $\eth^*(t) = \beta_d I^*(t) + \beta_i V^*(t) + d + \eta$ and $\Lambda_1^*(t) = \Lambda + \eta(N^*(t) - I^*(t))$. The periodicity of $S^*(t)$ implies that $S^*(t) > 0 \ \forall t \geq 0$. Also, $N(t) \geq S(t) \ \forall t \geq 0$ implies $N^*(t) > 0 \ \forall t \geq 0$. From (3.8) and (3.10), and the irreducibility of the cooperative matrix

$$\begin{pmatrix} \beta_d S^*(t) - \gamma - d & \beta_i S^*(t) \\ p & -\Omega(t) \end{pmatrix},$$

we get $(I^*(t), V^*(t)) \in \mathrm{Int}(\mathbb{R}^2_+) \ \forall t \geq 0$. Therefore, $(S^*(t), I^*(t), N^*(t), V^*(t))$ is a positive τ-periodic solution of system (3.7)–(3.10).

Acknowledgment. The authors are grateful to two anonymous referees for their insightful comments.

REFERENCES

[1] S. Akesson and A. Hedenstrom, *How migrants get there: Migratory performance and orientation*, BioScience, 52 (2007), pp. 123–133.

[2] T. Alerstam, *Conflicting evidence about long-distance animal navigation*, Science, 313 (2006), pp. 791–794.

[3] R. M. Anderson and R. M. May, *Infectious Diseases of Humans: Dynamics and Control*, Oxford University Press, Oxford, UK, 1991.

[4] D. M. Bates and D. G. Watts, *Nonlinear Regression Analysis and Its Applications*, Wiley, Hoboken, NJ, 2007.
[5] L. Bourouiba, A. Teslya, and J. Wu, *Highly pathogenic avian influenza outbreak mitigated by seasonal low pathogenic strains: Insights from dynamic modeling*, J. Theoret. Biol., 271 (2011), pp. 181–201.
[6] L. Bourouiba, J. Wu, S. Newman, J. Takekawa, T. Natdorj, N. Batbayar, C. Bishop, L. A. Hawkes, P. J. Butler, and M. Wikelski, *Spatial dynamics of bar-headed geese migration in the context of H5N1*, J. R. Soc. Interface, 7 (2010), pp. 1627–1639.
[7] R. Breban, J. M. Drake, and P. Rohani, *A general multi-strain model with environmental transmission: Invasion conditions for the disease-free and endemic states*, J. Theoret. Biol., 264 (2010), pp. 729–736.
[8] R. Breban, J. M. Drake, D. E. Stallknecht, and P. Rohani, *The role of environmental transmission in recurrent avian influenza epidemics*, PLoS Comput. Biol., 5 (2009), e1000346.
[9] J. D. Brown, D. E. Stallknecht, J. R. Beck, D. L. Suarez, and D. E. Swayne, *Susceptibility of North American ducks and gulls to H5N1 highly pathogenic avian influenza viruses*, Emerg. Infect. Dis., 12 (2006), pp. 1663–1670.
[10] J. D. Brown, D. E. Swayne, R. J. Cooper, R. E. Burns, and D. E. Stallknecht, *Persistence of H5 and H7 avian influenza viruses in water*, Avian Dis., 51 (2007), pp. 285–289.
[11] J. D. Brown, G. Goekjian, R. Poulson, S. Valeika, and D. E. Stallknecht, *Avian influenza virus in water: Infectivity is dependent on pH, salinity and temperature*, Vet. Microbiol., 136 (2009), pp. 20–26.
[12] K. P. Burnham and D. R. Anderson, *Model Selection and Multimodel Inference: A Practical Information-Theoretic Approach*, 2nd ed., Springer, New York, 2002.
[13] A. Cintron-Arias, C. Castillo-Chavez, L. M. A. Bettencourt, A. L. Lloyd, and H. T. Banks, *The estimation of the effective reproductive number from disease outbreak data*, Math. Biosci. Eng., 6 (2009), pp. 261–282.
[14] I. Davidson, S. Nagar, R. Haddas, M. Ben-Shabat, N. Golender, E. Lapin, A. Altory, L. Simanov, I. Ribshtein, A. Panshin, and S. Perk, *Avian influenza virus H9N2 survival at different temperatures and pHs*, Avian Dis., 54 (2010), pp. 725–728.
[15] M. A. De Marco, E. Foni, L. Campitelli, E. Raffini, M. Delogu, and I. Donatelli, *Long-term monitoring for avian influenza viruses in wild bird species in Italy*, Vet. Res. Commun., 27 (2003), pp. 107–114.
[16] O. Diekmann, J. A. Heesterbeek, and M. G. Roberts, *The construction of next-generation matrices for compartmental epidemic models*, J. R. Soc. Interface, 7 (2009), pp. 873–885.
[17] *Historical Climate Data*, http://www.climate.weatheroffice.gc.ca/climateData/canada_e.html.
[18] C. P. Farrington and H. J. Whitaker, *Estimation of effective reproduction numbers for infectious diseases using serological survey data*, Biostatistics, 4 (2003), pp. 626–632.
[19] *Climate Data*: *Finland*, http://www.tutiempo.net/en/Climate/Finland/FI.html (2010).
[20] S. R. Fereidouni, C. Grund, R. Hauslaigner, E. Lange, H. Wilking, T. C. Harder, M. Beer, and E. Starick, *Dynamics of specific antibody responses induced in mallards after infection by or immunization with low pathogenicity avian influenza viruses*, Avian Dis., 54 (2010), pp. 79–85.
[21] S. R. Fereidouni, E. Starick, M. Beer, H. Wilking, D. Kalthoff, C. Grund, R. Hauslaigner, A. Breithaupt, E. Lange, and T. C. Harder, *Highly pathogenic avian influenza virus infection of mallards with homo- and heterosubtypic immunity induced by low pathogenic avian influenza viruses*, PLoS One, 4 (2009), e6706.
[22] R. A. Fouchier, B. Olsen, T. M. Bestebroer, S. Herfst, L. van der Kemp, G. F. Rimmelzwaan, and A. D. Osterhaus, *Influenza A virus surveillance in wild birds in Northern Europe in* 1999 *and* 2000, Avian Dis., 47 (2003), pp. 857–860.
[23] R. A. Fouchier, V. Munster, A. Wallensten, T. M. Bestebroer, S. Herfst, D. Smith, G. F. Rimmelzwaan, B. Olsen, and A. D. Osterhaus, *Characterization of a novel influenza A virus hemagglutinin subtype (H16) obtained from black-headed gulls*, J. Virol., 79 (2005), pp. 2814–2822.
[24] T. L. Fuller, S. S. Saatchi, E. E. Curd, E. Toffelmier, H. A. Thomassen, W. Buermann, D. F. DeSante, M. P. Nott, J. F. Saracco, C. Ralph, J. D. Alexander, J. P. Pollinger, and T. B. Smith, *Mapping the risk of avian influenza in wild birds in the US*, BMC Infect. Dis., 10 (2010), 187.
[25] A. R. Gallant, *Nonlinear Statistical Models*, Wiley Ser. Probab. and Stat., Wiley, Hoboken, NJ, 1987.
[26] A. Germundsson, K. I. Madslien, M. J. Hjortaas, K. Handeland, and C. M. Jonassen, *Prevalence and subtypes of influenza A viruses in wild waterfowl in Norway* 2006-2007, Acta Vet. Scand., 52 (2010), 28.

[27] *The Weather in Cities in Germany*, http://www.tutiempo.net/en/Weather/Germany/DE.html (2010).
[28] S. A. Gourley, R. Liu, and J. Wu, *Spatiotemporal distributions of migratory birds: Patchy models with delay*, SIAM J. Appl. Dyn. Syst., 9 (2010), pp. 589–610.
[29] B. A. Hanson, D. E. Stallknecht, D. E. Swayne, L. A. Lewis, and D. A. Senne, *Avian influenza viruses in Minnesota ducks during* 1998–2000, Avian Dis., 47 (2003), pp. 867–871.
[30] J. R. Happold, I. Brunhart, H. Schwermer, and K. D. Stark, *Surveillance of H5 avian influenza virus in wild birds found dead*, Avian Dis., 52 (2008), pp. 100–105.
[31] V. Henaux, M. D. Samuel, and C. M. Bunck, *Model-based evaluation of highly and low pathogenic avian influenza dynamics in wild birds*, PLoS One, 5 (2010), e10997.
[32] V. S. Hinshaw, R. G. Webster, and B. Turner, *Water-bone transmission of influenza A viruses?*, Intervirology, 11 (1979), pp. 66–68.
[33] V. S. Hinshaw, R. G. Webster, and B. Turner, *The perpetuation of orthomyxoviruses and paramyxoviruses in Canadian waterfowl*, Can. J. Microbiol., 26 (1980), pp. 622–629.
[34] S. Huet, A. Bouvier, M. Poursat, and E. Jolivet, *Statistical tools for Nonlinear Regression: A Practical Guide with S-PLUS and R Examples*, Springer Ser. Statist., New York, (2003).
[35] H. S. Ip, P. L. Flint, J. C. Franson, R. J. Dusek, D. V. Derksen, R. E. Gill, Jr., C. R. Ely, J. M. Pearce, R. B. Lanctot, S. M. Matsuoka, D. B. Irons, J. B. Fischer, R. M. Oates, M. R. Petersen, T. F. Fondell, D. A. Rocque, J. C. Pedersen, and T. C. Rothe, *Prevalence of influenza A viruses in wild migratory birds in Alaska: Patterns of variation in detection at a crossroads of intercontinental flyways*, Virol. J., 5 (2008), 71.
[36] H. Kida, R. Yanagawa, and Y. Matsuoka, *Duck influenza lacking evidence of disease signs and immune response*, Infect. Immun., 30 (1980), pp. 547–553.
[37] E. D. Kilbourne, *Influenza pandemics of the* 20*th century*, Emerg. Infect. Dis., 12 (2006), pp. 9–14.
[38] S. Krauss, D. Walker, S. P. Pryor, L. Niles, L. Chenghong, V. S. Hinshaw, and R. G. Webster, *Influenza A viruses of migrating wild aquatic birds in North America*, Vector Borne Zoonotic Dis., 4 (2004), pp. 177–189.
[39] C. Lebarbenchon, C. M. Chang, S. van der Werf, J. T. Aubin, Y. Kayser, M. Ballesteros, F. Renaud, F. Thomas, and M. Gauthier-Clerc, *Influenza A virus in birds during spring migration in the Camargue, France*, J. Wildlife Dis., 43 (2007), pp. 789–793.
[40] L. Liu, X. Q. Zhao, and Y. Zhou, *A tuberculosis model with seasonality*, Bull. Math. Biol., 72 (2010), pp. 931–952.
[41] H. Lu and A. E. Castro, *Evaluation of the infectivity, length of infection, and immune response of a low-pathogenicity H*7*N*2 *avian influenza virus in specific-pathogen-free chickens*, Avian Dis., 48 (2004), pp. 263–270.
[42] R. I. Macey and D. F. Oster, *Berkeley Madonna*, Version 8.0. University of California at Berkley, 2001.
[43] V. J. Munster, C. Baas, P. Lexmond, J. Waldenstrom, A. Wallensten, T. Fransson, G. F. Rimmelzwaan, W. E. Beyer, M. Schutten, B. Olsen, A. D. Osterhaus, and R. A. Fouchier, *Spatial, temporal, and species variation in prevalence of influenza A viruses in wild migratory birds*, PLoS Patho., 3 (2007), e61.
[44] K. Okazaki, A. Takada, T. Ito, M. Imai, H. Takakuwa, M. Hatta, H. Ozaki, T. Tanizaki, T. Nagano, A. Ninomiya, V. A. Demenev, M. M. Tyaptirganov, T. D. Karatayeva, S. S. Yamnikova, D. K. Lvov, and H. Kida, *Precursor genes of future pandemic influenza viruses are perpetuated in ducks nesting in Siberia*, Arch. Virol., 145 (2000), pp. 885–893.
[45] B. Olsen, V. J. Munster, A. Wallensten, J. Waldenstrom, A. D. Osterhaus, and R. A. Fouchier, *Global patterns of influenza a virus in wild birds*, Science, 312 (2006), pp. 384–388.
[46] E. J. Parmley, N. Bastien, T. F. Booth, V. Bowes, P. A. Buck, A. Breault, D. Caswell, P. Y. Daoust, J. C. Davies, S. M. Elahi, M. Fortin, F. Kibenge, R. King, Y. Li, N. North, D. Ojkic, J. Pasick, S. P. Pryor, J. Robinson, J. Rodrigue, H. Whitney, P. Zimmer, and F. A. Leighton, *Wild bird influenza survey, Canada,* 2005, Emerg. Infect. Dis., 14 (2008), pp. 84–87.
[47] J. M. Pilgrim, X. Fang, and H. G. Stefan, *Stream temperature correlations with air temperatures in Minnesota: Implications for climate warming*, J. Amer. Water Res. Assoc., 34 (1998), pp. 1109–1121.
[48] L. A. Reperant, N. S. Fuckar, A. D. Osterhaus, A. P. Dobson, and T. Kuiken, *Spatial and temporal association of outbreaks of H*5*N*1 *influenza virus infection in wild birds with the* 0 *degrees C isotherm*, PLoS Pathog., 6 (2010), e1000854.

[49] B. Roche, C. Lebarbenchon, M. Gauthier-Clerc, C. M. Chang, F. Thomas, F. Renaud, S. van der Werf, and J. F. Guegan, *Water-borne transmission drives avian influenza dynamics in wild birds: The case of the* 2005–2006 *epidemics in the Camargue area*, Infect. Genet. Evol., 9 (2009), pp. 800–805.

[50] P. Rohani, R. Breban, D. E. Stallknecht, and J. M. Drake, *Environmental transmission of low pathogenicity avian influenza viruses and its implications for pathogen invasion*, Proc. Natl. Acad. Sci. USA, 106 (2009), pp. 10365–10369.

[51] S. H. Seo and R. G. Webster, *Cross-reactive, cell-mediated immunity and protection of chickens from lethal H5N1 influenza virus infection in Hong Kong poultry markets*, J. Virol., 75 (2001), pp. 2516–2525.

[52] G. B. Sharp, Y. Kawaoka, S. M. Wright, B. Turner, V. Hinshaw and R. G. Webster, *Wild ducks are the reservoir for only a limited number of influenza A subtypes*, Epidemiol. Infect., 110 (1993), pp. 161–176.

[53] H. L. Smith, *Monotone Dynamical Systems: An Introduction to the Theory of Competitive and Cooperative Systems*, Math. Surveys Monogr. 41, AMS, Providence, RI, 1995.

[54] H. L. Smith and P. Walman, *The Theory of the Chemostat*, Cambridge University Press, Cambridge, UK, 1995.

[55] D. E. Stallknecht, M. T. Kearney, S. M. Shane, and P. J. Zwank, *Effects of pH, temperature, and salinity on persistence of avian influenza viruses in water*, Avian Dis., 34 (1990), pp. 412–418.

[56] D. E. Stallknecht, S. M. Shane, M. T. Kearney, and P. J. Zwank, *Persistence of avian influenza viruses in water*, Avian Dis., 34 (1990), pp. 406–411.

[57] L. Subehi, T. Fukushima, Y. Onda, S. Mizugaki, T. Gomi, K. Kosugi, S. Hiramatsu, H. Kitahara, K. Kuraji, and T. Terajima, *Analysis of stream water temperature changes during rainfall events in forested watersheds*, Limnology, 11 (2010), pp. 115–124.

[58] L. Subehi, T. Fukushima, Y. Onda, S. Mizugaki, T. Gomi, T. Terajima, K. Kosugi, S. Hiramatsu, H. Kitahara, K. Kuraji, and N. Ozaki, *Influences of forested watershed conditions on fluctuations in stream water temperature with special reference to watershed area and forest type*, Limnology, 10 (2009), pp. 33–45.

[59] J. Suss, J. Schafer, H. Sinnecker, and R. G. Webster, *Influenza virus subtypes in aquatic birds of eastern Germany*, Arch. Virol., 135 (1994), pp. 101–114.

[60] H. R. Thieme, *Convergence results and a Poincaré-Bendixson trichotomy for asymptotically autonomous differential equations*, J. Math. Biol., 30 (1992), pp. 755–763.

[61] J. H. Tien and D. J. Earn, *Multiple transmission pathways and disease dynamics in a waterborne pathogen model*, Bull. Math. Biol., 72 (2010), pp. 1506–1533.

[62] P. van den Driessche and J. Watmough, *Reproduction numbers and sub-threshold endemic equilibria for compartmental models of disease transmission*, Math. Biosci., 180 (2002), pp. 29–48.

[63] K. K. Van Dalen, A. B. Franklin, N. L. Mooers, H. J. Sullivan, and S. A. Shriner, *Shedding light on avian influenza H4N6 infection in mallards: Modes of transmission and implications for surveillance*, PLoS One, 5 (2010), e12851.

[64] A. Wallensten, V. J. Munster, N. Latorre-Margalef, M. Brytting, J. Elmberg, R. A. Fouchier, T. Fransson, P. D. Haemig, M. Karlsson, A. Lundkvist, A. D. Osterhaus, M. Stervander, J. Waldenstrom, and O. Bjorn, *Surveillance of influenza A virus in migratory waterfowl in northern Europe*, Emerg. Infect. Dis., 13 (2007), pp. 404–411.

[65] W. Wang and X. Q. Zhao, *Threshold dynamics for compartmental epidemic models in periodic environments*, J. Dynam. Differential Equations, 20 (2008), pp. 699–717.

[66] R. G. Webster, M. Yakhno, V. S. Hinshaw, W. J. Bean, and K. G. Murti, *Intestinal influenza: Replication and characterization of influenza viruses in ducks*, Virology, 84 (1978), pp. 268–278.

[67] R. G. Webster, W. J. Bean, O. T. Gorman, T. M. Chambers, and Y. Kawaoka, *Evolution and ecology of influenza A viruses*, Microbiol. Rev., 56 (1992), pp. 152–179.

[68] *Cumulative Number of Confirmed Human Cases of Avian Influenza A/(H5N1) Reported to WHO*, http://www.who.int/csr/disease/avian_influenza/country/cases_table_2010_03_16/en/index.html (2010).

[69] L. Widjaja, S. L. Krauss, R. J. Webby, T. Xie, and R. G. Webster, *Matrix gene of influenza a viruses isolated from wild aquatic birds: Ecology and emergence of influenza A viruses*, J. Virol., 78 (2004), pp. 8771–8779.

[70] F. Zhang and X.-Q. Zhao, *A periodic epidemic model in a patchy environment*, J. Math. Anal. Appl., 325 (2007), pp. 496–516.

[71] X.-Q. Zhao, *Dynamical Systems in Population Biology*, Springer, New York, (2003).